Structures and Dynamics of Quasi-2D Mesoscale Convective Systems

MATTHEW D. PARKER

Department of Geosciences, University of Nebraska—Lincoln, Lincoln, Nebraska

RICHARD H. JOHNSON

Department of Atmospheric Science, Colorado State University, Fort Collins, Colorado

(Manuscript received 17 December 2002, in final form 2 October 2003)

ABSTRACT

Recently, three distinct archetypes for midlatitude linear mesoscale convective systems (MCSs) have been identified. This article focuses on the fundamentals of two of these archetypes: convective lines with trailing stratiform (TS) precipitation and convective lines with leading stratiform (LS) precipitation. Both the TS and LS modes typically exhibit quasi-2D reflectivity patterns and quasi-2D environmental storm-relative wind fields. Ongoing work has revealed that there are three common flow structures for these quasi-2D MCSs: *front-fed* TS systems (which are sustained by front-to-rear storm-relative inflow), as well as front-fed LS and *rear-fed* LS systems (which are sustained by rear-to-front storm-relative inflow). This paper summarizes the observed structures of the front-fed TS, front-fed LS, and rear-fed LS modes, and then outlines an idealized numerical experiment in which these modes were simulated. The authors analyze the basic simulated kinematic and microphysical structures and provide a framework in which to analyze the dynamics of the modeled systems. To a large degree, the organizational modes of developing quasi-2D MCSs may be anticipated by considering the magnitudes and preferred directions of the horizontal pressure gradient accelerations associated with a surface cold pool [whose strength is largely related to the environmental humidity and convective available potential energy (CAPE)] and an updraft in the mean environmental wind shear profile. In this regard, the lower-tropospheric shear is of prime importance, although the middle- and upper-tropospheric shear provide for additional, nontrivial accelerations.

1. Introduction

Mesoscale convective systems (MCSs) occur throughout large parts of the Americas (Laing and Fritsch 1997) and commonly produce severe weather (Fritsch and Forbes 2001). In particular, MCSs account for a disproportionate number of flash floods, and the degree to which they cause flooding is a function of their organizational modes and motion vectors (Doswell et al. 1996). Parker and Johnson (2000, hereafter abbreviated PJ00) investigated base scan reflectivity data from the central United States and cataloged 88 linear MCSs (i.e., convective systems possessing a convective line) that occurred over the course of 2 months. They found that, although the well-known convective line with trailing stratiform precipitation (TS) archetype accounted for roughly 60% of their study population, about 20% of the systems best corresponded to a convective line with leading stratiform precipitation (LS) archetype, and about 20% of the systems best corresponded to a convective line with parallel stratiform precipitation (PS) archetype. These archetypes are represented schematically in Fig. 1. The LS and PS modes have received very little attention to this point. Therefore, their dynamics and possibly unique internal structures are heretofore unexplored, which is surprising given their potential relevance to the flash flood forecast problem. As a first approach to this problem, the present study considers quasi-2D linear MCSs (the TS and LS modes), incorporating idealized numerical simulations in order to perform detailed analyses and test sensitivities. We set aside PS systems for later study owing to their three-dimensional complexity, which requires greater computer resources for simulation. This paper describes three common quasi-2D flow and precipitation structures among linear MCSs: *front-fed* TS systems (which are sustained by front-to-rear storm-relative inflow), as well as front-fed LS and *rear-fed* LS systems (which are sustained by rear-to-front storm-relative inflow).

Convective lines with leading precipitation pose several interesting questions that this paper addresses. First, given the ''mirror image similarity'' of their reflectivity fields to those of convective lines with trailing precipitation, just how similar are LS systems to TS systems dynamically and kinematically? PJ00 and Pettet and

Corresponding author address: Dr. Matthew Parker, 214 Bessey Hall, University of Nebraska—Lincoln, Lincoln, NE 68588-0340.
E-mail: parker@updraft.unl.edu

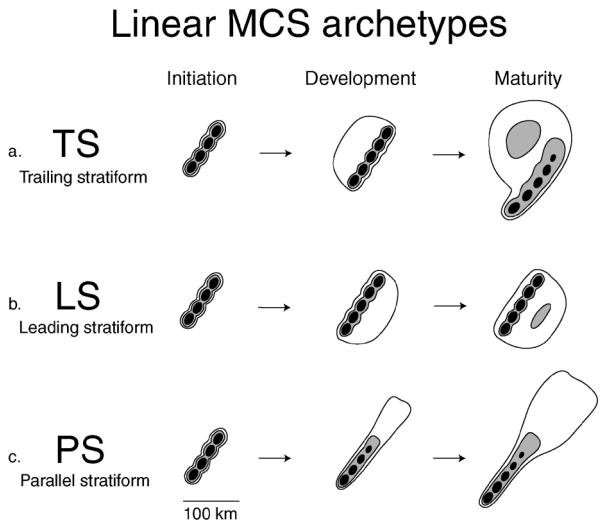

FIG. 1. Schematic reflectivity drawing of idealized life cycles for three linear MCS archetypes from Parker and Johnson (2000): (a) leading line with trailing stratiform precipitation; (b) convective line with leading stratiform precipitation; (c) convective line with parallel stratiform precipitation. Approximate time interval between phases: for TS, 3–4 h; for LS, 2–3 h; for PS, 2–3 h. Levels of shading roughly correspond to 20, 40, and 50 dBZ.

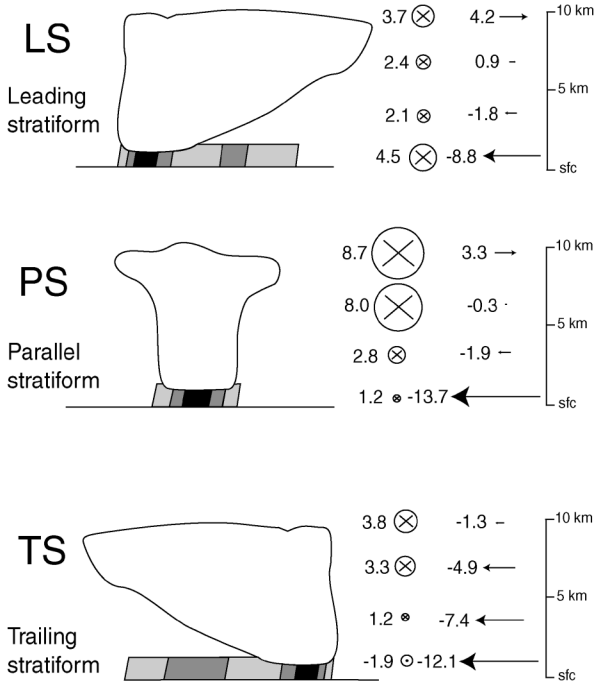

FIG. 2. Vertical profiles of layer-mean storm-relative pre-MCS winds for linear MCS classes from Parker and Johnson (2000). Wind vectors depicted as line-parallel (⊗) and line-perpendicular (→) components (m s^{-1}). Layers depicted are 0–1, 2–4, 5–8, and 9–10 km. Typical base scan radar reflectivity patterns (shading) and hypothetical cloud outlines are drawn schematically for reference. MCSs' leading edges are to the right.

Johnson (2003) found in case studies that at least some of the LS systems in the central United States are sustained by inflow of high-θ_e air from behind the system (i.e., they were rear fed). However, the mean wind profiles computed by PJ00 revealed that, on average, the LS systems in their study were chiefly front fed[1] (Fig. 2). Indeed, a significant number of the individual LS systems in that population were front fed. Hence, the LS reflectivity category must be understood to comprise at least two kinematic subtypes: front-fed LS (FFLS) systems, as well as rear-fed LS (RFLS) systems. For completeness, we note that all of the TS systems PJ00 investigated were front fed, hence the additional term front-fed TS (FFTS) MCS is also appropriate. In many ways, RFLS systems do indeed possess mirror image similarity to FFTS systems. This paper describes their similarities and details their few relevant differences. Notably, FFLS systems are distinctly different from FFTS and RFLS systems, a point that this paper introduces.

a. Background

The rich body of literature concerning squall lines and linear convective systems traces its lineage primarily through significant papers about FFTS systems, especially those by Newton (1950), Ogura and Liou (1980), Smull and Houze (1985), Smull and Houze (1987), Rutledge et al. (1988), and Houze et al. (1989). The common attributes of these FFTS systems are described further in section 2a. The above-mentioned studies, along with countless others, led to the unifying paper by Houze et al. (1990), in which the authors specified criteria for the FFTS archetype and assessed the degree to which a large population of Oklahoma convective systems met those criteria. In turn, the paper by Houze et al. (1990) was one among several that constitute a lineage of taxonomy papers, including those by Bluestein and Jain (1985), Blanchard (1990), and Schiesser et al. (1995). Standing on the shoulders of these many studies, PJ00 investigated 88 linear MCSs from the central United States and classified them as either TS, LS, or PS [a taxonomy similar to that of Schiesser et al. (1995), for Swiss MCSs]. The present work about quasi-2D systems is the latest effort in a string of papers on the structures, kinematics, and dynamics of convective systems—especially FFTS convective systems—that is more than half of a century old.

Meanwhile, as studies of FFTS MCSs were gaining a literary critical mass, other papers that addressed systems with some FFLS characteristics sporadically appeared, including those by Newton and Fankhauser

[1] Although not shown, wind profiles from *behind* LS MCSs in the Parker and Johnson (2000) study also did not reveal [within the resolution of the National Oceanic and Atmospheric Administration (NOAA) profiler network] mean rear-to-front storm-relative flow. In other words, the LS MCS population was apparently not, on average, rear fed.

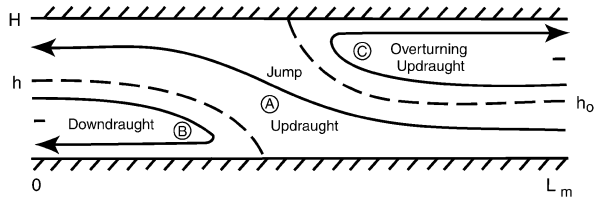

FIG. 3. Schematic diagram of the airflow in Moncrieff's (1992) stationary dynamical model for two-dimensional convection.

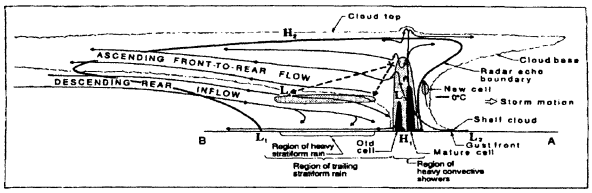

FIG. 4. Conceptual model from Houze et al. (1989) of front-fed convective line with trailing (stratiform) precipitation, viewed in a vertical cross section oriented perpendicular to the convective line and parallel to its motion.

(1964), Houze and Rappaport (1984), Kessinger et al. (1987), and Fankhauser et al. (1992). Recent papers by Grady and Verlinde (1997) and Nachamkin et al. (2000) have shed some additional light on FFLS systems, and section 2c of this paper gives more detailed attention to their results. In contrast to these front-fed systems, an LS case presented by PJ00 also showed that some convective lines with leading precipitation are likely fed by rear-to-front inflow from behind their convective lines (i.e., they are RFLS systems); this configuration is similar to those discussed by Maddox et al. (1979) for mesohigh-type flash floods and by Fritsch et al. (1994) for convective regeneration near slowly moving mesovortices. Pettet and Johnson (2003) endorsed the basic interpretation that RFLS systems are kinematically similar to reversed (mirrored) FFTS systems, although they noted several unique features of the RFLS systems that they studied. Section 2b of this paper summarizes the common kinematic features of the RFLS mode.

Thorpe et al. (1982) summarized a 2D numerical simulation with a conceptual model that comprised an overturning updraft, a rearward-sloping jump updraft, an up–down rearward-flowing airstream (with a possible rotor), and an overturning downdraft. This fit well with an idealized theoretical model that they derived, which is depicted in Fig. 3 [as redrawn by Moncrieff (1992)]. As shown in Moncrieff's (1992) Fig. 2 (not reproduced here), the steady-state transport properties of any 2D convective line can be idealized by considering slight modifications and asymptotic limits to the basic structure in Fig. 3. In the parameter space that Moncrieff (1992) discussed, the jump updraft might be more or less prominent than that shown in Fig. 3, and might occur without either an overturning updraft or an overturning downdraft. As section 2 will show, the FFLS mode fits well with the theoretical case in which the overturning updraft is predominant, whereas both the FFTS and RFLS modes fit well with the theoretical case in which the jump updraft is predominant.

Unfortunately, prior studies have not been able to fully address the possible dynamical similarities and differences between the RFLS and FFTS archetypes. As well, the differences between RFLS and FFLS systems were not appreciated because of their similar reflectivity patterns. The present study addresses them separately, comparing their dynamics to those of FFTS systems, and thereby spanning the entire spectrum of quasi-2D convective systems. Numerical simulations are ideal for this pursuit owing to their suitability for various kinds of controlled experiments, which have enabled us to describe important environmental factors and their effects on convective organization. In addition to their suitability for sensitivity tests, numerical simulations also provide gridded, high-resolution results that represent ideal datasets with which to investigate dynamical hypotheses. In addition to the physical interpretations that Seitter and Kuo (1983), Nicholls et al. (1988), Weisman et al. (1988), and Szeto and Cho (1994) proposed as a result of their sensitivity tests, other authors (e.g., Yang and Houze 1995; Fovell and Tan 1998; Lin et al. 1998) have advanced the dynamical understanding of squall lines by performing idealized 2D simulations. The present work is descended from the above ancestries of numerical studies in that it comprises sensitivity tests for simulated convective systems and in that it seeks to learn about convective dynamics by analyzing the high-resolution model output.

b. Structure of this paper

Section 2 reviews observations and summarizes the common traits of the three quasi-2D MCS modes. Section 3 then describes the basic setup of the numerical model that we used for this study, as well as our methods of analysis. Thereafter, section 4 presents results from numerical simulations of quasi-2D convective systems, and section 5 synthesizes and interprets the observations and simulations of the three quasi-2D modes. The paper concludes with some possible directions for future work and a brief summary.

2. Common observations of quasi-2D MCSs

a. Front-fed TS systems

The basic flow structures for convective lines with trailing precipitation are fairly well documented. Archetypally, as Houze et al. (1989) outlined (see Fig. 4 of the present paper), FFTS systems possess deep convective cells that are fed by front-to-rear storm-relative flow in the lower troposphere, which partly ascends and weakly overturns, but which mostly exits the convective region with some part of its front-to-rear momentum remaining. After leaving the convective region, humid

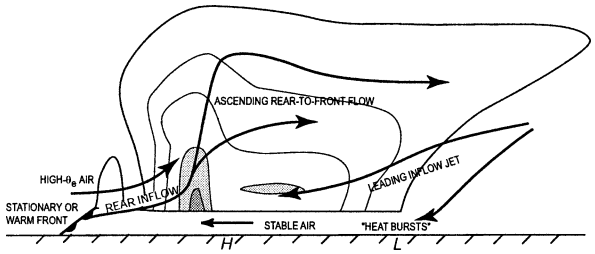

FIG. 5. Conceptual model, from Pettet and Johnson (2003), of a rear-fed convective line with leading precipitation, viewed in a vertical cross section oriented perpendicular to the convective line and parallel to its motion.

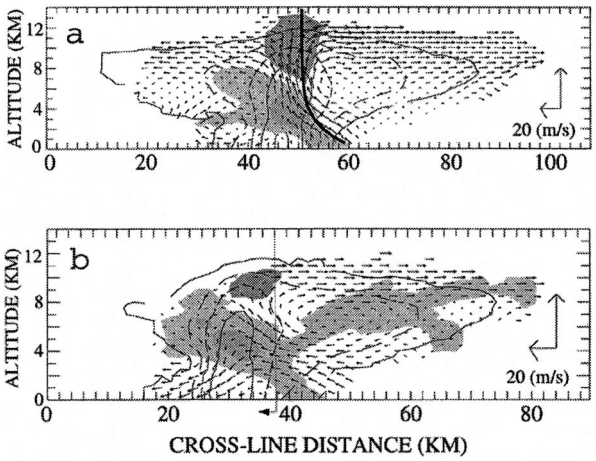

FIG. 6. Along-line averaged cross sections at two times for squall line from Grady and Verlinde (1997), at (a) 2102 UTC and (b) 2131 UTC 21 Jun 1993. Reflectivity contours are in 10-dBZ increments beginning with 10 dBZ. Vectors depict line-relative flow. Light shading indicates convergence, dark shading indicates divergence.

air and activated hydrometeors move rearward, comprising a zone into which liquid and ice particles are advected and in which continued condensational and depositional growth occurs; this becomes the trailing precipitation region. Small upward accelerations owing to any remaining buoyancy from the convective region, in addition to contributions from in situ latent heating, render modest ascent in the front-to-rear flow stream (Fig. 4). Beneath the region of middle and upper troposphere positive buoyancy, a quasi-static pressure minimum develops (as labeled L_4 in Fig. 4) in response to which environmental air from behind the system may be accelerated inward and begin to constitute a rear inflow jet. Owing largely to melting, evaporation, and sublimation of the precipitation that falls into this rear inflow jet, as well as hydrometeor loading, downward accelerations accumulate in this airstream and commonly render a descending slope to it (Fig. 4). These flow features have been repeatedly observed within FFTS MCSs and, in addition to the well-known FFTS reflectivity signature, may be considered a basic benchmark of success for numerical simulations of FFTS systems.

b. Rear-fed LS systems

Although observations of RFLS systems are notably less common in the literature than those of FFTS systems, Pettet and Johnson (2003) considered several archetypal cases and produced a schematic composite depiction of their structure (Fig. 5). The predominant flow branches, although reversed with respect to the system's orientation and direction of motion, are notably similar to those of the archetypal FFTS system (Fig. 4). Rather than a front-to-rear airstream that feeds the convective line and then slopes upward and rearward to generate the trailing precipitation region of the FFTS system, Fig. 5 depicts the common arrangement of a rear-to-front airstream that feeds the convective line and then slopes upward and forward to generate the leading precipitation region of the RFLS system. Owing to similar microphysical and dynamical processes, a descending jet of front-to-rear flow occurs in the RFLS system which is a mirror image counterpart to the descending rear-inflow jet of the FFTS system. The work of Pettet and Johnson (2003) therefore suggests that, in terms of reflectivity and mesoscale flow structures, the RFLS archetype corresponds for the most part to a reversed FFTS system. The flow features depicted in Fig. 5 may be considered a basic benchmark of success for numerical simulations of RFLS systems. And, as a result of their general similarity, resemblance to other common aspects of FFTS systems could also be interpreted as symptoms of a proper RFLS MCS simulation. However, as the analysis in later sections demonstrates, there are dynamical reasons to expect FFTS and RFLS systems to differ in some basic, although perhaps difficult to observe, ways.

c. Front-fed LS systems

Although FFLS systems have appeared in the literature, there has not yet been a thorough description of their commonalities. Presented here are vertical cross sections depicting the quasi-2D reflectivity and wind structures of two FFLS systems: a system from 21 June 1993, as analyzed by Grady and Verlinde (1997) and shown here in Fig. 6, and an archetypal system from the original PJ00 population that passed over St. Louis, Missouri, on 4 May 1996, as shown in Fig. 7. In both cases, a deep convective line was preceded by a large overhanging region of line-leading precipitation. For the 4 May system, the line-leading precipitation had appreciable reflectivity very near the surface (Fig. 7a), as measured by the lowest radar scan. For the 21 June system, a somewhat less archetypal FFLS example, little precipitation appears to have reached the ground more than 20 km ahead of the convective line. Both examples exhibited deep (at least 0–5 km AGL) front-to-rear storm-relative inflow that passed through their line-lead-

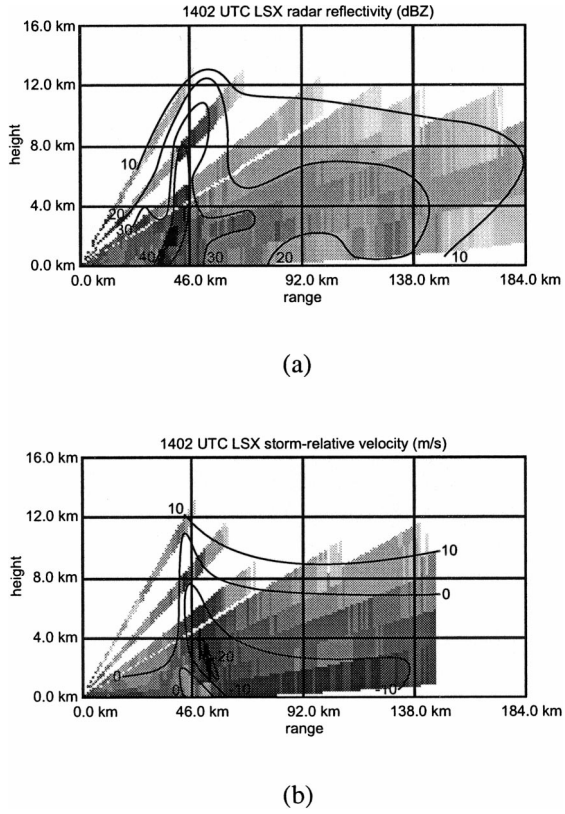

FIG. 7. Vertical range-height cross sections of a front-fed convective line with leading precipitation from St. Louis (LSX) radar at 1402 UTC 4 May 1996, azimuth 110° (a) Reflectivity (dBZ), (b) storm-relative velocity (m s^{-1}) using a storm motion of 20 m s^{-1} parallel to the cross section. Measured data are plotted, with subjectively analyzed contours added manually.

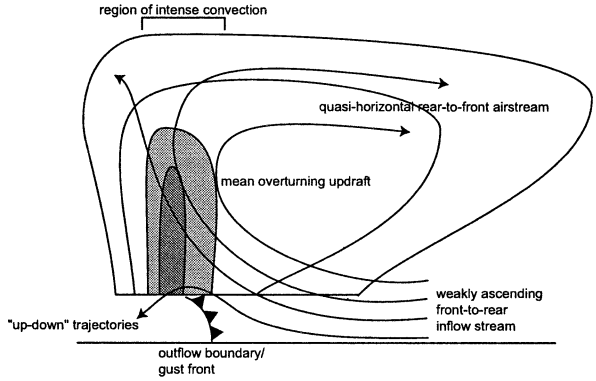

FIG. 8. Conceptual model, based on compiled radar observations, of a front-fed convective line with leading precipitation, viewed in a vertical cross section oriented perpendicular to the convective line and parallel to its motion.

ing precipitation. Also, the vectors in Fig. 6 and the contours in Fig. 7b suggest that their inflowing airstreams ascended slightly as they traversed the preline precipitation. The wind vectors in Fig. 6 reveal a deep overturning updraft, which can also be inferred from the reflectivity and storm-relative flow fields in Fig. 7. Both examples also suggest that some air in the front-to-rear stream ascended near the surface gust front and then descended and joined the surface cold pool (the cold pool head and gust front in Fig. 7b are evinced by a region of stagnant flow near range = 46 km). Finally, both examples exhibited a strong, roughly horizontal stream of rear-to-front flow in the middle and upper troposphere. Much as the ascending front-to-rear flow branch in FFTS systems and the ascending rear-to-front flow branch in RFLS systems, this rear-to-front airstream in FFLS systems appears to be the predominant source of humidity and hydrometeors for the line-leading precipitation region. Another example from 19 July 1993, described by Nachamkin et al. (2000), also shared these properties. These basic, common kinematic and reflectivity attributes suggest a third, simple schematic diagram for FFLS systems as shown in Fig. 8, which, along with Figs. 4 and 5, stands to complete the set of benchmarks for simulated quasi-2D MCSs. We consider similarity to the common aspects of FFLS systems as depicted in Fig. 8 to signal a realistic RFLS MCS simulation.

3. Methods

a. Numerical simulations

This paper makes use of idealized numerical simulations to describe the basic evolutions and dynamics of quasi-2D mesoscale convective systems. Numerical modeling techniques are desirable for attacking this problem owing to their suitability for sensitivity tests and the paucity of high-resolution observations (e.g., dual-Doppler wind fields) available for large sets of in-depth case studies. This work incorporated both 2D and 3D simulations using version 4.5.2 of the Advanced Regional Prediction System (ARPS), a fully compressible nonhydrostatic model developed by the Center for Analysis and Prediction of Storms (CAPS) and the University of Oklahoma. The dynamical framework of the ARPS was described by Xue et al. (1995, 2000, 2001). For the sake of brevity, in this paper we only outline the model settings and results for the 2D simulations. The 3D simulations were performed on coarser grids but essentially affirmed the results of the 2D simulations.

In order to explicitly simulate convective clouds on the domain, the 2D simulations had grid spacings of 1 km. Trial and error revealed that a domain size of 600 km in the across-line dimension (for this study, $\hat{x}$) was large enough to simulate MCSs without having the lateral boundary conditions add appreciable error. The domain height was 18 km, having rigid, free-slip conditions on both the upper and lower boundaries, and a Rayleigh damping layer in the model stratosphere (the uppermost 6 km of the domain). The vertical grid in the model was stretched, with an averaged spacing of

499 m, ranging from 250 m in the lowest 2 km of the domain to 730 m in the stratosphere of the 2D simulations. The simulations incorporated implicit differencing in $\hat{z}$ and used a large timestep of 3.5 s and a small (acoustic) timestep of 1.75 s. The model used a 1.5-order turbulence kinetic energy (TKE)-based closure. In order to damp very short waves and prevent instabilities on the domain, the model also included fourth-order computational mixing, an Asselin time filter, and divergence damping. The model's $\hat{x}$ lateral boundaries (the eastern and western edges) had a wave-radiating (open) boundary condition. The control simulations did not include Coriolis accelerations, radiative effects, or surface fluxes. The simulations used a six-category water microphysics scheme (including ice) based on those from Tao and Simpson (1993) and Lin et al. (1983).

Much as Yang and Houze (1995), Weisman et al. (1997), and others have done, in order to initiate convection, the model included an initial surface cold box that was 2 km deep, extended from the downstream boundary to the center of the domain, and had a constant buoyancy of -0.2 m s^{-2} (which corresponds to a potential temperature perturbation of -6.4 K in the base-state sounding). This was the minimal cold pool strength that reliably initiated a long-lived convective system in all of the idealized wind profiles. For this study, a cold box was preferable to warm thermals because it mimics the way that convective lines tend to be initiated in the real world: 63 of the 64 linear warm-sector MCSs studied by PJ00 occurred at or near a linear surface boundary (e.g., front, pressure trough, dryline, or outflow boundary). In addition, the long linear edge of the cold box was useful in the 3D simulations (not shown) for ensuring that the convective line's initial orientation with respect to the wind profile was correct.

b. Two-dimensionality and quasi-2D MCSs

This study addressed systems that are *quasi 2D*, meaning that toward their centers their flow almost exclusively lies in line-perpendicular planes. Although we performed numerous 2D and periodic-3D simulations, for the sake of brevity we present only results from the 2D simulations in section 4. Several experiments revealed that the central regions of long but finite 3D convective lines behave much like 2D and periodic-3D lines. This is particularly true of cases in the present study, for which the typical environmental wind profiles are nearly 2D (i.e., the LS and TS profiles in Fig. 2) and for which convection is often initiated by a long linear boundary. The strong similarity of the 2D numerical results to observed real-world precipitation and kinematic structures, as well as the strong correspondence of the sensitivities and mean structures between the 2D and nonperiodic 3D simulations, suggest that the physical insights gained from the following 2D simulations are both fairly applicable to the real world phenomena and fairly robust.

One relevant concern in using 2D and periodic-3D simulations is that interesting and potentially important line-end effects, such as those simulated by Skamarock et al. (1994), are lost. However, the present study focuses on the line-perpendicular structure of convective systems' quasi-2D regions, which are generally in the lines' centers and far from the lines' ends. We do not wish to understate the importance of line-end effects, but in this case we wish to focus on the development and structure of the quasi-2D interior line sections. Another valid concern is that periodic boundary conditions in $\hat{y}$ place an unnecessary quasi-2D constraint upon gravity wave dispersion. However, this constraint likely exists to some degree in the middle sections of long quasi-2D convective lines in the real world because, when heating occurs over a line's entire length, gravity waves' along-line flux divergences in the center of the line become quite small. Several tests incorporated open boundary conditions on the northern and southern edges of the domain. Overall, the simulated convection's structure and evolution were not affected much by changing the $\hat{y}$ boundary condition, probably because the simulations never developed large v-wind components. Therefore, it appears that the use of a periodic condition in $\hat{y}$ did not overly detract from the results of this study. A third concern with the method in this study is that the control runs' initial states included no v wind. However, sensitivity tests indicated that the inclusion of a realistic v wind did not substantially affect the structure or evolution of the periodic 3D simulations. Finally, basic theory and prior modeling results demonstrate that quasi-supercellular convective modes often develop in high-shear regimes. Two dimensions are clearly inadequate for simulating supercellular convection. At this point, it must suffice to say that our fully 3D simulations in typical FFLS wind profiles, which approach marginal shear values for supercells, did indeed produce quasi-2D FFLS MCSs. We set aside other 3D structures in high-shear regimes for another study.

c. Means for dynamical analysis

Because numerical model output comprises gridded, high-resolution data for all pertinent variables, it is possible to carry out a more detailed analysis than with the conventional observations presented in the previous section. Of particular interest in this study were the horizontal accelerations experienced by air passing through the systems' convective regions. Invoking anelasticity and scaling the equations of motion by assuming that density perturbations are small compared to the mean, one obtains the flux form for the equations of motion:

$$\frac{\partial}{\partial t}(\rho_0 \mathbf{u}) = \boldsymbol{\nabla} \cdot (\rho_0 \mathbf{u}\mathbf{u}) + \boldsymbol{\nabla} p' + 2\rho_0 \boldsymbol{\Omega} \times \mathbf{u} - \rho_0 \mathbf{B} = 0, \quad (1)$$

wherein all variables have their conventional meanings, $\mathbf{B} \equiv -\mathbf{g}\rho'/\rho_0$ for brevity of notation, and frictional decelerations have been omitted. Taking $\nabla\cdot(1)$, and neglecting the Coriolis terms as small for convective-scale analysis, the diagnostic pressure equation for the anelastic set is [cf. Wilhelmson and Ogura (1972), e.g.]

$$\nabla^2 p' = -\nabla\cdot[\rho_0(\mathbf{u}\cdot\nabla)\mathbf{u}] + \frac{\partial}{\partial z}(\rho_0 B). \tag{2}$$

The diagnostic pressure equation is then typically (e.g., Rotunno and Klemp 1982) decomposed into buoyant and dynamic components ($p' = p'_B + p'_D$):

$$\nabla^2 p'_B = \frac{\partial}{\partial z}(\rho_0 B); \tag{3}$$

$$\nabla^2 p'_D = \underbrace{-\rho_0\left[\left(\frac{\partial u}{\partial x}\right)^2 + \left(\frac{\partial v}{\partial y}\right)^2 + \left(\frac{\partial w}{\partial z}\right)^2 - w^2\frac{\partial^2}{\partial z^2}(\ln\rho_0)\right]}_{\text{extension terms}}$$
$$\underbrace{-2\rho_0\left(\frac{\partial v}{\partial x}\frac{\partial u}{\partial y} + \frac{\partial u}{\partial z}\frac{\partial w}{\partial x} + \frac{\partial v}{\partial z}\frac{\partial w}{\partial y}\right)}_{\text{shear terms}}. \tag{4}$$

Following Klemp (1987), the extension terms imply maximized pressure in regions of nonzero divergence or deformation, and the shear terms imply minimized pressure in regions of nonzero vorticity. It is of further interest to diagnose the linear and nonlinear parts of the dynamic pressure perturbation: the linear part represents the simple dynamical effects of the environment on a convective eddy, whereas the nonlinear part represents the more complicated effects of local and mesoscale wind perturbations. Analysis of the linear and nonlinear parts is accomplished by considering that the base-state wind profile in the simulations is 2D, such that the wind components can be decomposed as $u = u_0(z) + u'$, $v = v'$, and $w = w'$. The linear part of (4) is therefore

$$\nabla^2 p'_{\rm DL} = -2\rho_0\frac{du_0}{dz}\frac{\partial w}{\partial x}. \tag{5}$$

The nonlinear part of the dynamic pressure perturbation ($p'_{\rm DNL}$) is then simply $p'_D - p'_{\rm DL}$. Using this decomposition, $p'_{\rm DL}$ accounts for the component of the pressure maximum on an updraft's upshear side and the pressure minimum on an updraft's downshear side that are solely attributable to the presence of the mean environmental shear; $p'_{\rm DNL}$ accounts for all of the remaining dynamical effects.

Using the above pressure decomposition, the irrotational equation for motion can be written

$$\underbrace{\frac{D\mathbf{u}}{Dt}}_{\text{ACC}} = \underbrace{\underbrace{-\frac{1}{\rho_0}\nabla p'_B}_{\text{BUOY}} \underbrace{-\mathbf{g}\left(\frac{\rho'_{\rm gas}}{\rho_0}\right)}_{\text{DRAG}}}_{\text{ACCB}} \underbrace{-\frac{1}{\rho_0}\nabla p'_{\rm DL}}_{\text{ACCDL}} \underbrace{-\frac{1}{\rho_0}\nabla p'_{\rm DNL}}_{\text{ACCDNL}}, \tag{6}$$

wherein $\rho'_{\rm gas}$ is the density perturbation attributable to the gaseous constituents and q_h is the total hydrometeor mixing ratio. In words, BUOY is the acceleration owing to local buoyancy of humid air, DRAG is the acceleration owing to the weight of hydrometeors suspended in the air, ACCB is the acceleration owing to the combined effects of local buoyancy and the gradient in the buoyant pressure field, ACCDL is the acceleration owing to the gradient in the linear dynamic pressure field, and ACCDNL is the acceleration owing to the gradient in the nonlinear dynamic pressure field. ACC is the total parcel acceleration owing to the sum of ACCB, ACCDL, and ACCDNL, implicitly neglecting contributions by acoustic waves, which are presumably unimportant.

d. Base-state wind profiles

The mean environmental wind profiles for midlatitude FFTS systems generally possess a predominantly line-perpendicular wind shear vector directed from rear-to-front (e.g., in Fig. 2). The same is also true of the three RFLS case studies presented by PJ00 and Pettet and Johnson (2003). The difference, of course, is that the convective line is on an FFTS system's downshear side (in this study, the eastern side), but on an RFLS system's upshear side (in this study, the western side). As an additional caveat, the wind profiles from PJ00's case (their Fig. 16) and at least one of the soundings from Pettet (2001)'s work (her Fig. 5.4a) show lower tropospheric jet profiles for RFLS cases, with reverse shear thereabove, hereafter abbreviated as ''RFLS-jet.'' Fritsch et al. (1994) also identified a similar jet profile in a rear-fed system. The present study addressed the basic dynamics of convective systems in these three flow regimes, plus the FFLS regime, by incorporating five simulations using the simple wind profiles in Fig. 9. These wind profiles are storm relative, and were iteratively adjusted by adding a constant to keep the simulated systems centered within the model domain. Al-

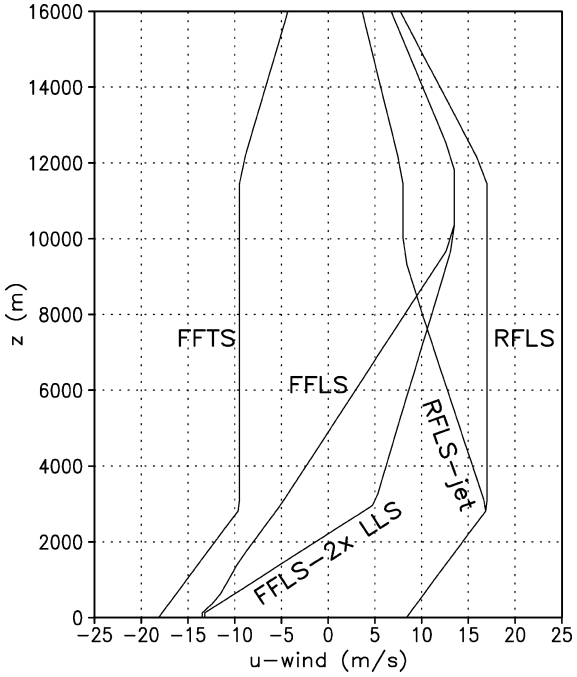

FIG. 9. Profiles of u wind used in the idealized numerical experiments. The FFTS and RFLS profiles are identical to one another within the troposphere, save for an added constant.

though the wind profiles in Fig. 9 are highly idealized, they are useful because they permit a more controlled experiment. The FFTS and RFLS profiles are identical to one another in the troposphere (to within an added constant); they therefore completely isolate the role of the lower-tropospheric shear vector's orientation with respect to the outflow boundary. A simultaneous simulation of both an FFTS system on a cold pool's eastern edge and an RFLS system on that cold pool's western edge (not shown) confirmed the correctness of this approach. The simulations with the RFLS-jet profile included an additional simple reverse shear layer above 3 km AGL, in order to address the possible importance of the middle- and upper-tropospheric shear in RFLS-jet cases. Finally, the simplest FFLS wind profile was identical to the RFLS and FFTS profiles from 0–3 km AGL, but maintained the linear wind shear of that layer all the way up to 10 km AGL. In this respect, it has identical low-level shear (LLS) but increased deep layer shear compared to the RFLS and FFTS profiles. In order to evaluate the importance of the low-level shear we also created an FFLS–2xLLS profile in which the 0–3-km shear was doubled, the 3–10-km shear halved, but the 0–10-km shear remained constant. Archetypal FFLS systems from the PJ00 study generally had wind profiles falling somewhere between these extremes.

e. Base-state soundings

The model had a horizontally homogeneous initial condition, which was defined by a single sounding. The environmental temperature and humidity sounding for this study was manually interpolated between the mean sounding for 59 warm-sector MCSs from PJ00 and the mean sounding for 42 classifiable systems from Houze et al. (1990), as shown in their Fig. 15; therefore, it resembled those for midlatitude MCSs. Notably, except for their lowest 2 km, the two mean soundings were nearly identical to one another. In both studies, the soundings utilized were the best available conventional, operational observations, which were not always very close to the convective system in time and/or space. Accordingly, the averaged soundings in both studies, and in the new sounding for the present work, had significant convective inhibition (CIN, whose magnitude was generally $\geq$100 J kg^{-1}) and did not exhibit deep surface mixed layers. This is likely because many of the soundings were from 1200 UTC (early morning in North America) and had not been destabilized by diurnal heating. Therefore, the present study used an artificial, 1-km-deep surface mixed layer for the mean sounding incorporating the mean sounding's maximal values of θ and q_v from the lowest 1 km.

In practice, empirically determined analytic functions [closely following the structure used by Weisman and Klemp (1982)] defined the sounding used in the simulations. This was beneficial because the analytic functions were easy to modify in order to change the sounding systematically. The resulting sounding, as shown by the heavy solid line in Fig. 10, is slightly smoothed but is nevertheless representative of the mean environment for midlatitude linear MCSs. This control, mean MCS sounding is hereafter called CTRL. The bulk thermodynamic variables that describe the mean MCS sounding are summarized in Table 1. Although this mean sounding is deemed to represent a typical midlatitude MCS's environment, it did not permit long-lived convection to be initiated in the idealized RFLS and RFLS-jet simulations. Accordingly, we developed two modifications to it so that we could compare common cases within one consistent thermodynamic environment but with different wind profiles. In neither case did we modify the temperature profile. However, in the first alteration we increased the humidity of the sounding by increasing the surface mixing ratio from 15 to 20 g kg^{-1} and increasing the middle tropospheric relative humidity from 35% to 65%. This sounding, shown by the medium-weight dotted line in Fig. 10, is hereafter called MOIST. The MOIST sounding was considerably more humid and had much more convective available potential energy (CAPE) than the original (4290 versus 2577 J kg^{-1}). In these modified simulations entrainment had a less detrimental effect on updrafts, and updrafts were generally stronger owing to the environment's greater potential buoyancy. In the second alteration, meant to mimic the common observation of elevated high θ_e in the RFLS systems' rear inflow, we preserved the equivalent potential temperature of the low levels and allowed this constant-θ_e layer to extend upward until the relative

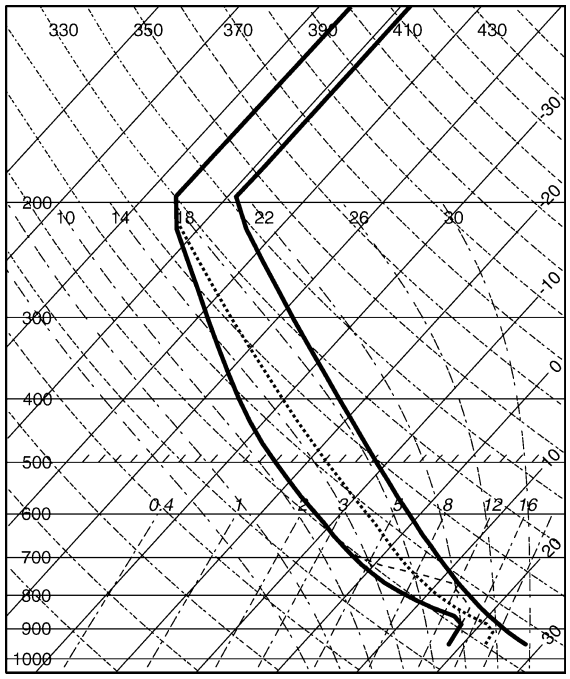

FIG. 10. Skew*T*–log*p* diagram of the mean MCS sounding used in this study, along with two modifications (described in the text). The control, mean MCS sounding (CTRL) is plotted with thick solid curves. The humidity profile for the moistened sounding (MOIST, with $q_{sfc} = 0.22$ and $r_{min} = 0.65$) is plotted with a medium-weight dotted curve. The humidity profile for the deepened θ_e maximum sounding (DEEP) is plotted with a thin-dashed line. Bulk thermodynamic variables for the CTRL sounding are given in Table 1.

humidity was 95% (shown by the thin-dashed line in Fig. 10). Thereabove, the relative humidity was held fixed at 95% up to 2 km AGL, and then relaxed back to that of the original sounding. This second modification thereby possessed the same surface-based CAPE as the original sounding, but had higher θ_e in the 1–2-km layer, from which we hypothesized that the convection might be fed. We only used this ''deepened θ_e maximum'' sounding, hereafter called DEEP, with the RFLS and RFLS-jet wind profiles.

Notably, the CAPE for these soundings is on the high end of typical values for midlatitude MCSs as documented by Houze et al. (1990) and PJ00. However, as discussed above, the original mean sounding had to be modified in order for convection to be initiated and survive in the simulations; presumably, nature also destabilizes the environment (removing CIN and adding CAPE) prior to real world convective initiation. There may be subsynoptic-scale augmentation in many cases that evades detection and is not represented in our averaged sounding. It may also be that, in real-world cases, there exist processes that compensate for low-CAPE/high-CIN environments in ways that are not captured by our idealized experiments.

TABLE 1. Bulk thermodynamic variables for the analytic mean MCS sounding. Parcel indices are computed using an unmixed surface air parcel.

Thermodynamic parameter	Value
Lifting condensation level (hPa)	840
Level of free convection (hPa)	795
Convective available potential energy (J kg^{-1})	2577
Convective inhibition (J kg^{-1})	−34
Lifted index (K)	−8.4
Precipitable water (cm)	3.20

4. Simulations of quasi-2D MCSs

a. FFTS and RFLS simulations

In case studies, PJ00 and Pettet and Johnson (2003) noted the mirror image resemblance of several rear-fed LS systems to front-fed TS systems. Additionally, Parker et al. (2001) noted some gross similarities in their patterns of cloud-to-ground lightning. However, given the relatively coarse observational data that were used for those studies, it was unclear to those authors how similar were the dynamics of RFLS and FFTS systems. This section compares and contrasts the basic mesoscale features that occur in simulated 2D FFTS and RFLS systems, which occur at opposite ends of a surface cold pool for a given wind profile.

1) OVERVIEW OF SIMULATED STRUCTURES

Although Hovmöller diagrams of 3 km AGL total hydrometeor mixing ratio (q_h) provide only limited insight into the actual structures and dynamics of the FFTS and RFLS convective systems, they are important in that they bridge the gap between base scan radar data and the present simulations. The horizontal shape and evolution of the 2D FFTS and RFLS simulations are summarized in Fig. 11. They dovetail with the quasi-2D structures that PJ00 documented, and correspond well with the basic reflectivity fields suggested by Figs. 4 and 5. In both cases, convection develops near the edge of the initial cold pool trigger and then begins to spread hydrometeors increasingly downwind over the cold pool (rearward in the FFTS case, forward in the RFLS case). The cellular patterns in the Hovmöller diagrams are an artifact of the plotting software and data output interval (9 min); the wavelike horizontal structure results from updrafts and downdrafts propagating away from the gust front in the quasi-stationary systems. The RFLS system in Fig. 11c also shows evidence of westward backbuilding, facilitated by the upwind spreading of the cold pool as it was reinforced by convective outflow. Notably, in the MOIST sounding (which had increased CAPE), updrafts were more intense. As a result, the MOIST FFTS simulation produced more hydrometeors and a broader stratiform region (cf. Figs. 11a and 11b), and thereby a stronger cold pool; as a result, the system accelerated forward later in its lifetime. As mentioned earlier, no long-lived RFLS

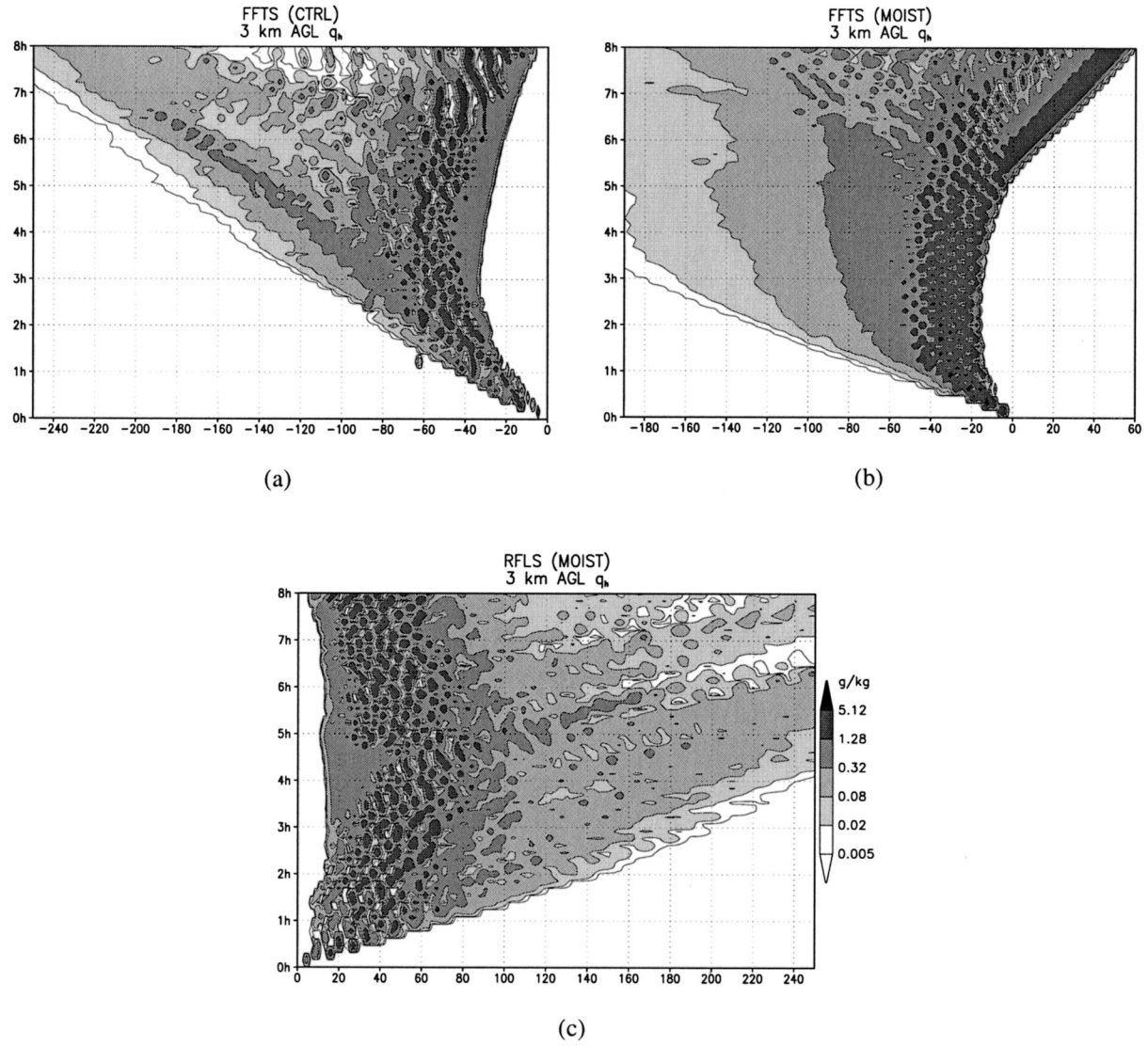

FIG. 11. Hovmöller diagram depicting 3-km-AGL hydrometeor mixing ratio (from $t = 0$–8 h, with an output frequency of 9 min) for (a) FFTS simulation with CTRL sounding and (b) FFTS and (c) RFLS simulations with MOIST sounding. Levels of shading are 0.005, 0.02, 0.08, 0.32, 1.28, and 5.12 g kg^{-1}.

system occurred in the CTRL simulation, so we only present the RFLS MOIST simulation results for comparison to the FFTS simulations.

Temporally averaged (from 9828–17 472 s, approximately 2 h,44 min–4 h,51 min cross sections through the moistened FFTS and RFLS simulations (Fig. 12) reveal basic system-scale kinematic features that are also consistent with those discovered by prior observational studies (Figs. 4 and 5), including deep middle- and upper-tropospheric conveyors (from front to rear in the FFTS case; rear to front in the RFLS case) and lower to middle-tropospheric pressure minima within their stratiform regions. Therefore, to the degree that these simulated systems are relatives of real world FFTS and RFLS systems, it is worthwhile to investigate their dynamical similarities and differences.

2) GOVERNING DYNAMICS

In many respects, the Hovmöller diagrams of q_h for the FFTS and RFLS simulations do indeed have mirror image similarity (Fig. 11). Because the only initial difference between the FFTS and RFLS simulations is the side of the cold pool on which the convection is initiated, it is fairly easy to describe the dynamical differences between the simulations in the early going. After 546 s (9.1 min), the initial updrafts produced in the two simulations are quite different from one another (Fig. 13). By this time, the FFTS system has produced a healthy updraft (with $w > 12$ m s^{-1}) that extends upward to approximately 5 km AGL (Fig. 13a). Meanwhile, the RFLS simulation has produced a weak updraft ($w < 4$ m s^{-1}) that slopes strongly downshear and has little

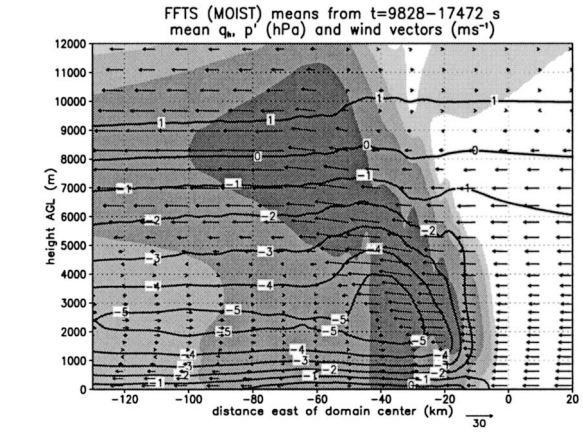

(a)

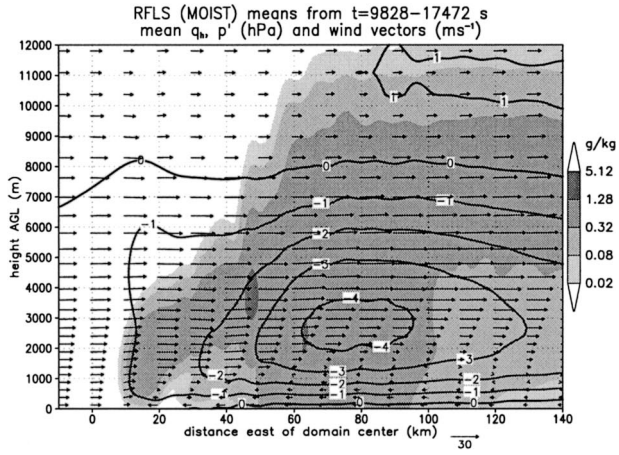

(b)

FIG. 12. Mean total hydrometeor mixing ratio (levels of shading are 0.02, 0.08, 0.32, 1.28, and 5.12 g kg^{-1}), pressure perturbation (contours, hPa), and ground-relative wind vectors (m s^{-1}, scaled as shown) for (a) FFTS and (b) RFLS simulations with MOIST sounding. Averaging is from 9828–17 472 s (approximately 2 h,44 min–4 h,51 min).

vertical extent (Fig. 13b). Much as shown by Moncrieff and Liu (1999), the edge of the cold pool is steeper on its downshear (i.e., Fig. 13a) than on its upshear (i.e., Fig. 13b) side.

To understand why the simulations are so different by $t = 546$ s, it is useful to analyze the accelerations in the very early going, at $t = 119$ s (Figs. 14 and 15). In both cases, ACCB is initially almost identical (Figs. 14c and 15c), as it should be given the two simulations' identical initial cold pool shapes and strengths. ACCB generates a rotor with time, accelerating the cold air toward the outflow boundary and the inflowing air upward, and then rearward in the FFTS case (forward in the RFLS case) and downward. In turn, this rotor is associated with a minimum in p'_{DNL} that adds to these rearward (forward in the RFLS case) and downward accelerations as air passes over it (Figs. 14d and 15d). However, the upward ACCB at the edge of the cold pool, which increases with height over the lowest 1 km AGL, renders a maximum in w at approximately 1.5 km AGL as inflowing air parcels move through the forcing (Figs. 14a and 15a). In the presence of a mean shear, this causes p'_{DL} to be most perturbed around 1.5 km AGL (Figs. 14e and 15e). In both simulations, this induces an eastward ACCDL that increases with height at and on the warm side of the outflow boundary (Figs. 14e and 15e). This counteracts the rearward ACCB and renders a more erect updraft and cold-air nose in the FFTS simulation, but adds to the forward ACCB and renders a more sloped updraft and cold-air nose in the RFLS simulation.

In time, the differing slopes of the cold air's nose feed back into the process because the steeper outflow boundary in the FFTS case produces deeper lifting via ACCB than does the shallow wedge of cold air in the RFLS case. The more upright cold pool nose in the FFTS case causes a more rapid deceleration of the inflow in the lowest 1 km AGL, yielding a zone of stronger convergence and a low-level maximum in p'_{DNL} that can also aid in accelerating inflow upward (this is already weakly present at $x = -1$ to $+1$ km in Fig. 14d). Finally, as the more erect outflow boundary in the FFTS simulation produces a stronger gust front updraft, p'_{DL} increases and the downshear ACCDL further assists the updraft's development by giving air parcels more upright trajectories and allowing them to spend more time in the zone of deep upward forcing as they move through it. In contrast, any contribution from ACCDL in the RFLS simulation will only accelerate the air parcels more strongly forward. These accumulated differences in ACCDL, ACCB, and ACCDNL result in the significant disparity between the FFTS and RFLS simulations by $t = 546$ s (Fig. 13).

In the above acceleration framework, the prime difference is that, in the FFTS case, the downshear ACCDL produces a more upright gust front updraft because it opposes the combined rearward ACCB and ACCDNL, both of which are attributable to the cold pool's pressure field. In contrast, in the RFLS case, ACCDL acts in the same direction as ACCB and ACCDNL, rendering a strong forward slope to the gust front updraft. Or, with reference to Rotunno et al.'s (1988) horizontal vorticity (η) framework, η of the environmental air parcels and $D\eta/Dt$ owing to the cold pool are opposite-signed for the FFTS system (which they call ''optimal'' for deep lifting), but same-signed for the RFLS system (which they would not call optimal).

As a result of this basic dynamical dissimilarity, the vertical cross sections through the FFTS and RFLS systems reveal important differences (Fig. 12). The

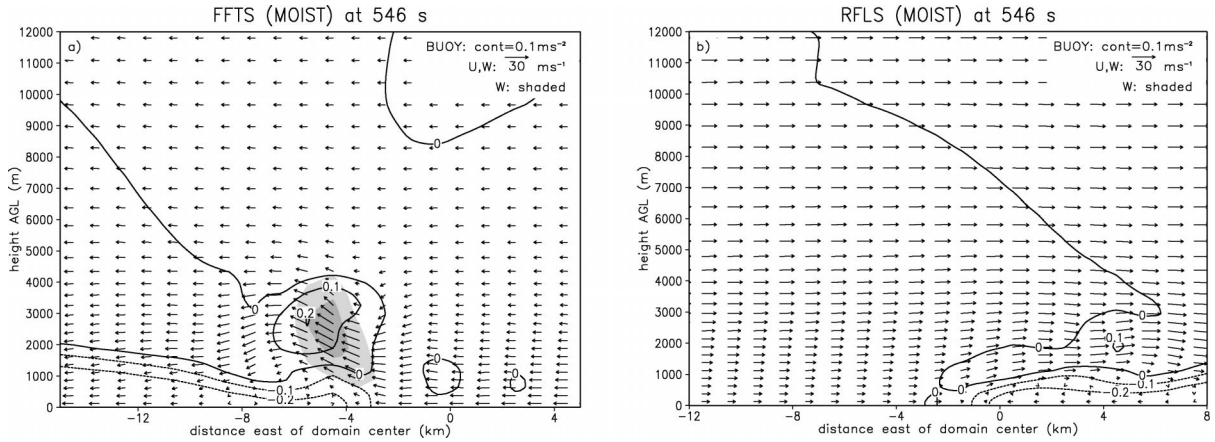

FIG. 13. Buoyancy and wind vectors at $t = 546$ s for (a) FFTS (MOIST) and (b) RFLS (MOIST) simulations. Vertical velocity shaded at 5 and 10 m s^{-1}. Contour intervals and vector scales are shown for each.

updrafts in the FFTS simulation are, on average, stronger than those in the RFLS simulation. Indeed, it is difficult to see any mean upward motion for the RFLS case in Fig. 12b. As a result of the stronger updrafts and mesoscale ascent in the FFTS system, the vertically integrated hydrometeor content is much greater than in the RFLS simulation (cf. Figs. 12a and 12b), even though their 3-km-AGL q_h Hovmöller diagrams look fairly similar to one another. Implicit in the greater condensate load for the FFTS system is that more latent heating has occurred, and hence the stratiform precipitation region contains more buoyancy. A symptom of this buoyancy is that the mesoscale quasi-hydrostatic p'_B field is more perturbed in the FFTS system (the temporally averaged pressure perturbations in Fig. 12 are almost entirely attributable to p'_B, not shown): the midlevel minimum in p' is about 1 hPa lower than that in the RFLS system (cf. Figs. 12a and 12b), the cloud-top maximum in p' is about 1 hPa higher than that in the RFLS system, and the horizontal pressure gradient around 2–3 km AGL is much larger than in the RFLS system (cf. Fig. 12a, $x = -30$ to $x = -10$ km versus Fig. 12b, $x = 10$ to $x = 60$ km). Whereas the lack of strong localized w and the broad shallow slope of the q_h field in the RFLS system (Fig. 12b) imply gradual ascent as air moves forward, with a concomitant quasi-horizontal buoyancy field, the localized maximum in w and the erect column of maximized q_h in the FFTS system imply steeper ascent of the rearward flow, with a concomitant increase in the slope of the buoyancy field. Hence, the sharp gradient in p' for the FFTS case is largely attributable to the more erect buoyancy field of its ascending airstream. The FFTS case maintains its more upright stature through maturity despite the additional rearward ACCB that this minimum in p'_B imposes on updraft air.

3) RFLS-JET: IMPACT OF REVERSE SHEAR

The Hovmöller diagram of 3-km-AGL q_h for the RFLS-jet MOIST simulation (Fig. 16a) was similar to that for the base RFLS MOIST case (Fig. 11c). And, because their 0–3-km wind profiles were identical and the convection in both simulations was initiated on the upshear side of the initial cold pool, their low-level dynamics and evolution in the early going were almost identical (not shown). However, the temporally averaged vertical cross section through the mature RFLS-jet system (Fig. 17) reveals that its structure lies somewhere between the RFLS and mirror image FFTS extremes. In particular, the mean w is slightly larger in the RFLS-jet simulation (although this is hard to see in Fig. 17), the hydrometeor content is greater and the pressure field is correspondingly more perturbed. Although a deep plume of significant w is still not evident in Fig. 17, the q_h field is more erect, and analysis of the RFLS-jet system's temporally varying fields revealed that individual updrafts were indeed more erect. The only difference between the RFLS and RFLS-jet simulations is the addition of the reverse shear aloft in the RFLS-jet environment. Therefore, the prime dynamical reason for the more upright structure in the RFLS-jet system is the westward ACCDL owing to the existence of easterly shear above 3 km AGL. The front-to-rear ACCDL aloft in the RFLS-jet simulations compensates in part for the rear-to-front ACCDL in low levels. Given the observations of jet profiles by PJ00 and Pettet and Johnson (2003), the middle- and upper-tropospheric ACCDL may be an important dynamical component in rendering more upright convection in real-world RFLS systems such as documented by Pettet and Johnson (2003). Fritsch et al. (1994) also noted the importance of this reverse shear layer above low-level jets, and discussed the dynamics of such rear-fed systems in a horizontal vorticity framework.

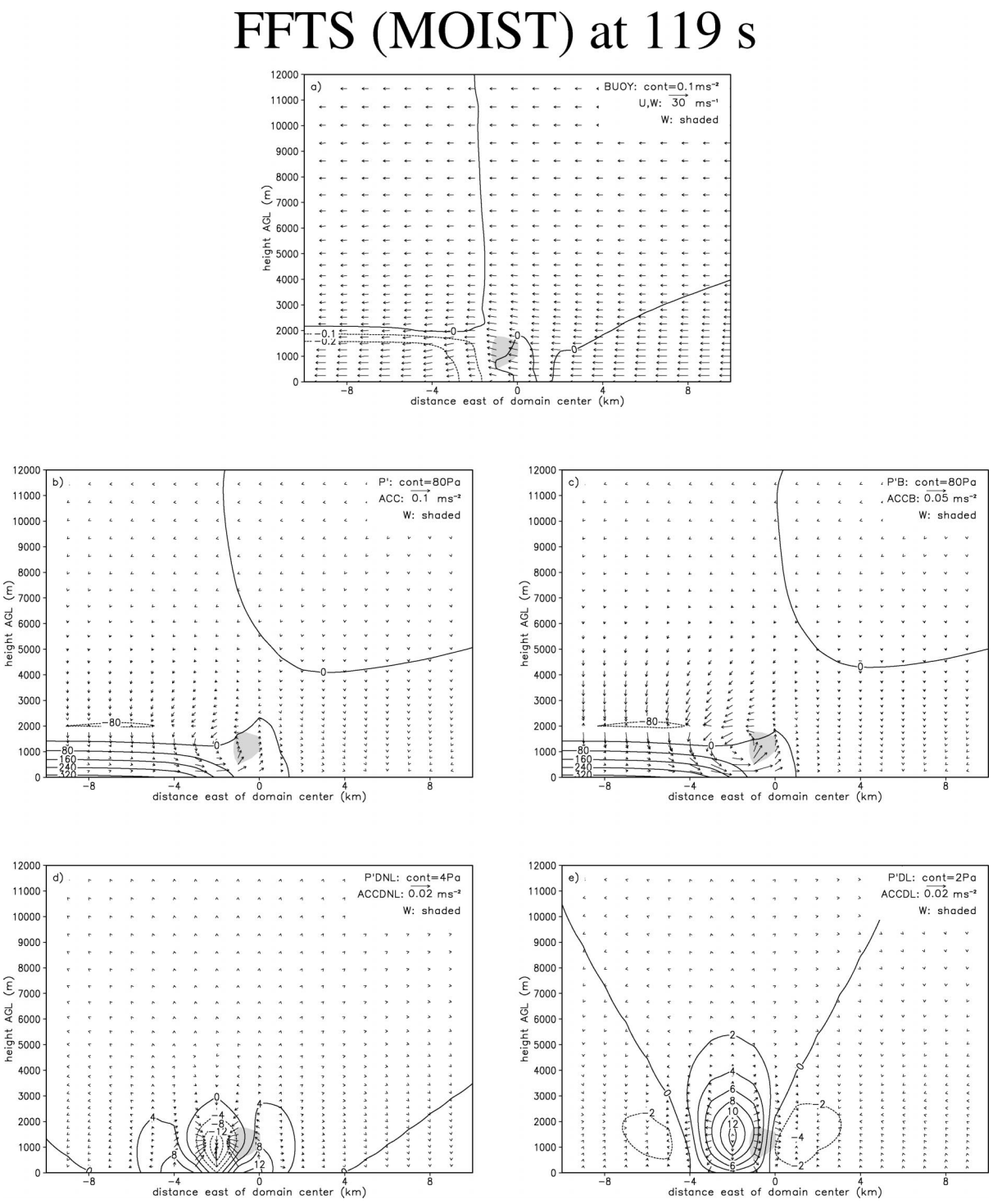

FIG. 14. Velocities, perturbation pressures, and acceleration terms for simulation FFTS (MOIST) AT 119 s. (a) BUOY contoured, u and w vectors; (b) p' contoured, ACC vectors; (c) p'_B contoured, ACCB vectors; (d) p'_{DNL} contoured, ACCDNL vectors; (e) p'_{DL} contoured, ACCDL vectors. Vertical velocity is shaded; levels of shading are 3 and 6 m s^{-1}. Contour intervals and vector scales are shown for each, and vary among (a)–(e). Abbreviations for terms are as defined in section 3c.

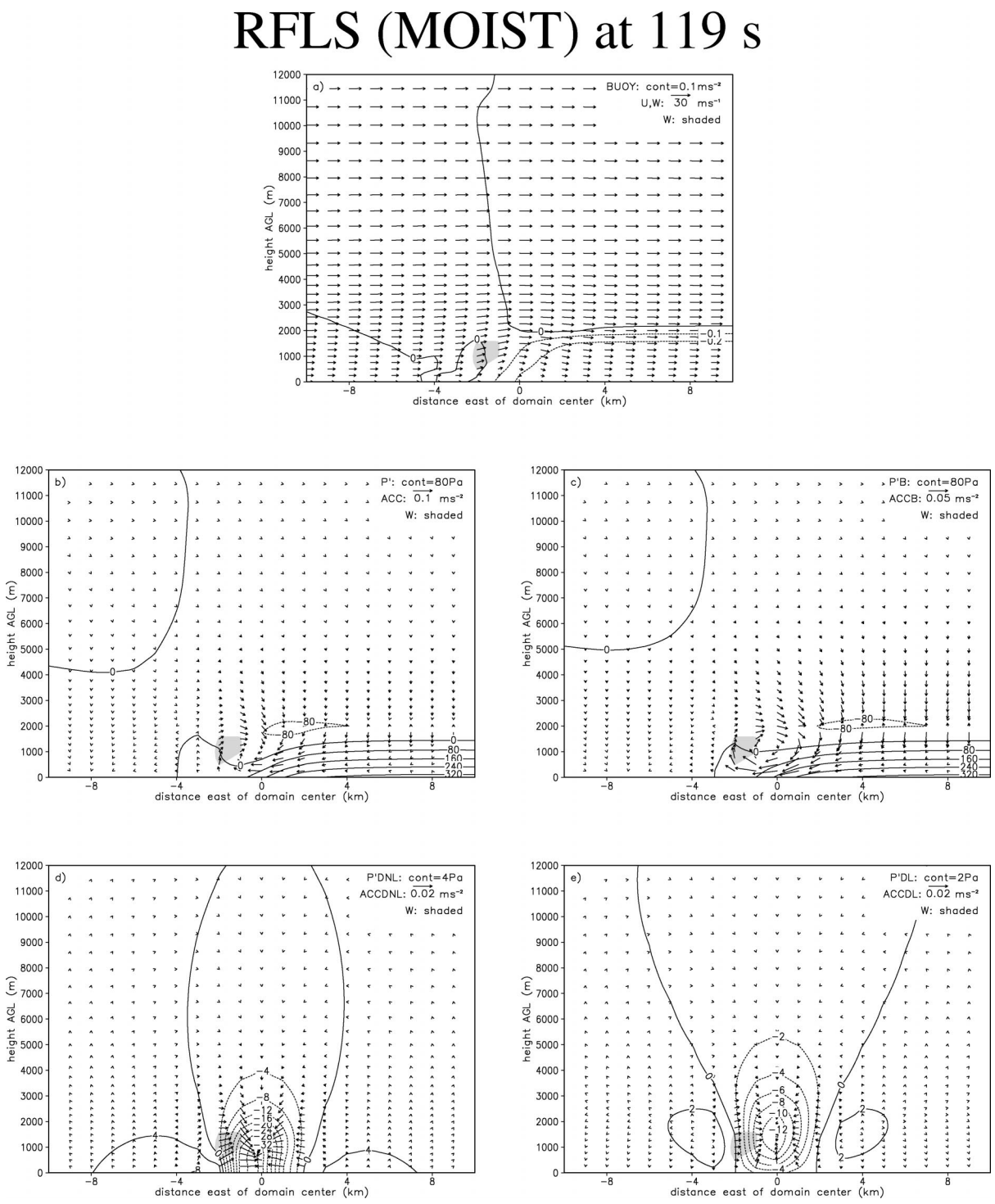

FIG. 15. Same as Fig. 14, but for simulation RFLS (MOIST) at 119 s.

The presence of increased θ_e values in the 1-2-km-AGL layer of the DEEP sounding (as compared to the CTRL sounding) did enable a long-lived RFLS system to develop in the RFLS-jet wind profile, although not in the original RFLS profile (in that case the convection was less organized and produced little stratiform precipitation). The properties of the RFLS-jet system in the DEEP sounding were similar to those of the RFLS-jet system in the moistened profile, although the stratiform region was smaller and total hydrometeor content

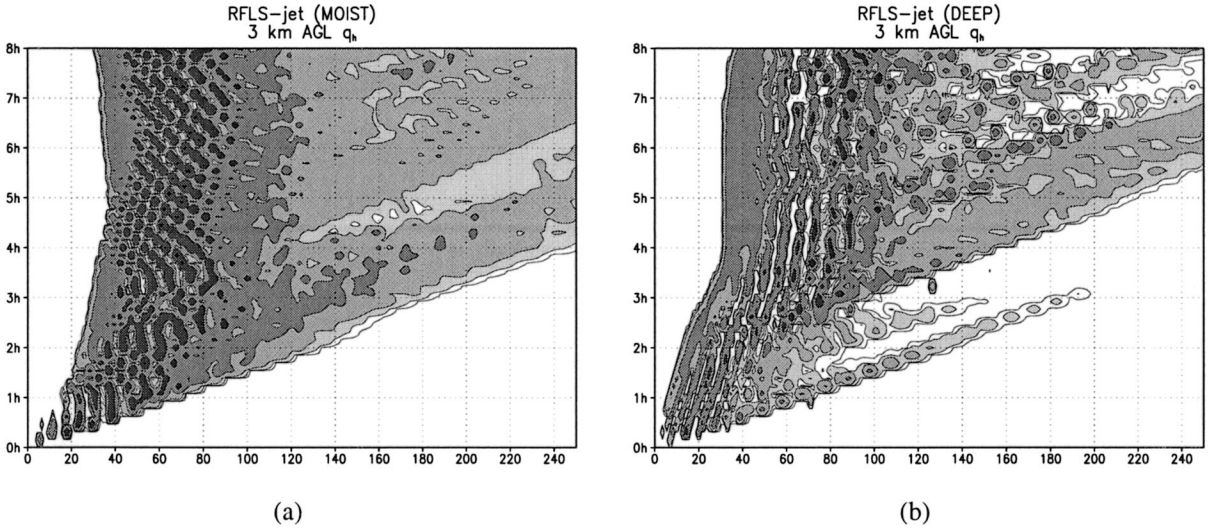

FIG. 16. Same as Fig. 11, but for RFLS-jet simulations with (a) MOIST sounding and (b) DEEP sounding.

lower owing to the lower CAPE and middle- and upper-tropospheric relative humidity. Nevertheless, the RFLS-jet case in the DEEP environment is consistent with the hypothesis that, without changing surface-based CAPE or CIN, the presence of an elevated θ_e maximum may enhance the likelihood of a long-lived RFLS system, particularly in conjunction with a low-level jet. This elevated high-θ_e air has CAPE and may escape much of the detrimental downshear acceleration in the lowest 1 or 2 km AGL. Notably, both PJ00 and Pettet and Johnson (2003) found that the highest-θ_e rear-to-front inflow for some RFLS systems was not rooted in the boundary layer. Because these systems were mostly nocturnal, the near-surface boundary layer was generally stable, and the systems updrafts were likely ingesting air from the remnants of the previous day's convectively mixed boundary layer. In addition, horizontal transports by a low-level jet could further increase the local θ_e above the nocturnal stable layer. Such scenarios are somewhat too complicated for the idealized modeling approach of the present study. However, it is quite possible that elevated θ_e maxima are important to the basic processes of RFLS systems. As suggested by Pettet and Johnson (2003), additional studies with fine-scale thermodynamic observations and dual-Doppler radar data are needed to resolve the local details of this potentially important process. Numerical simulations of RFLS systems using more realistic midlatitude nocturnal boundary layers would also shed more light on the problem.

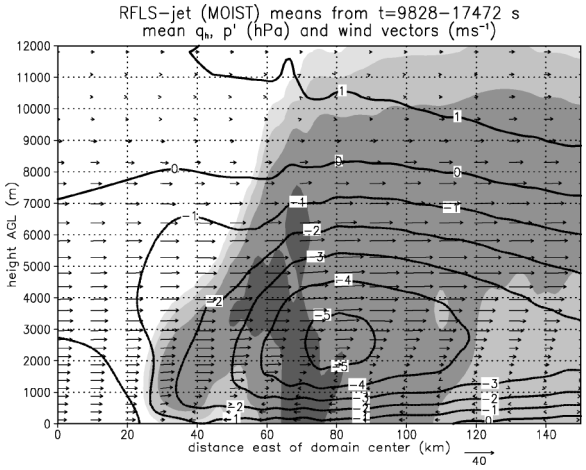

FIG. 17. Same as Fig. 12, but for RFLS-jet simulation with MOIST sounding.

b. FFLS simulations

1) OVERVIEW OF SIMULATED STRUCTURES

The idealized simulations of FFLS systems were generally marked by several features. First, although all of the FFLS simulations initially produced line-leading precipitation, all of the FFLS simulations also evolved toward FFTS structure with time (Fig. 18). The CTRL sounding FFLS simulation evolved to FFTS structure the most rapidly and is not shown in detail in this paper. The other three simulations (FFLS–2xLLS with the CTRL sounding, and both FFLS and FFLS–2xLLS in the MOIST sounding) evolved much less rapidly toward FFTS structure and continued to produce line-leading precipitation throughout the first 8 h of the simulations. The FFLS–2xLLS wind profile produced something akin to an archetypal real-world FFLS system in the CTRL simulation, as summarized by Figs. 18a and 19a. The leading precipitation region developed with time throughout the first 3 h of the simulation, eventually attaining a quasi-stable size. Its mean cross section

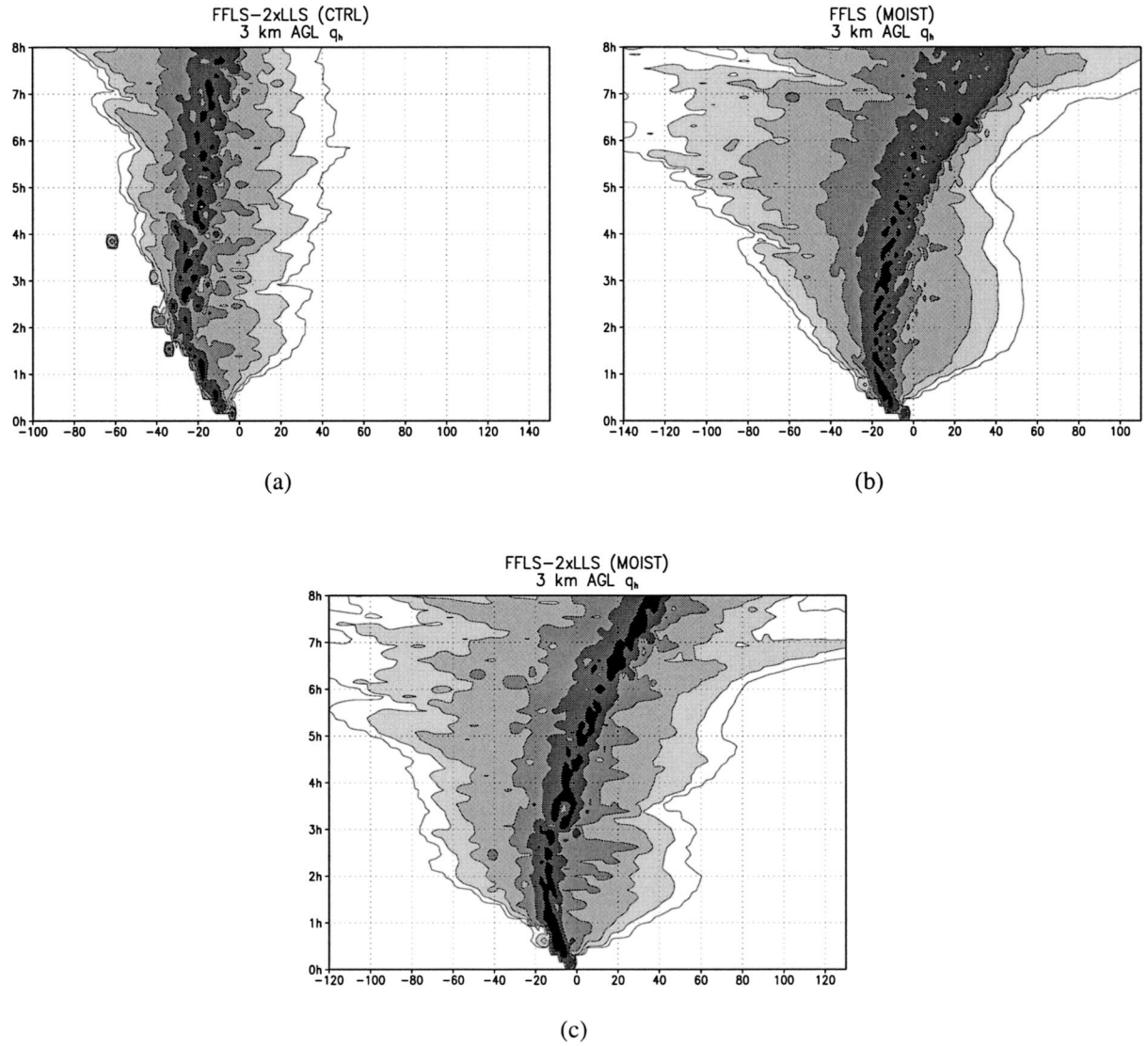

FIG. 18. Same as Fig. 11, but for (a) FFLS–2xLLS simulation with CTRL sounding and (b) FFLS and (c) FFLS–2xLLS simulations with MOIST sounding.

(Fig. 19a) depicts a precipitation structure and predominant overturning updraft that are quite consistent with the archetypal model extracted from observations (Fig. 8). In this section we present results from the FFLS–2xLLS CTRL simulation, since they most closely conform to the archetypal model, but also refer to the FFLS and FFLS–2xLLS MOIST results as a basis for comparison to the FFTS and RFLS simulations. The impact of doubling the low-level shear is discussed later. The impact of using the MOIST (instead of CTRL) sounding is similar to that discussed for the FFTS cases: a much greater hydrometeor load is generated in the high-CAPE MOIST regime, and as a result the surface cold pool intensifies more rapidly.

In the FFLS simulations, deep convection was continually initiated above the surface cold pool in the vicinity of its outflow boundary. Despite the vigorous convection feeding water vapor and condensate into the line-leading precipitation region, surface rainfall rates >1 mm h^{-1} extended only 20–25 km ahead of the convective line on average in the simulated FFLS systems (can be inferred from Figs. 18–19). There appears to be some observational support for this result: in reviewing the PJ00 study data, as well as the cases in Figs. 6 and 7, it became clear that many of the observed FFLS cases had comparatively smaller stratiform regions than their RFLS (or FFTS) cousins. The present simulation results are consistent with these data in that the simulated FFTS systems do indeed have larger trailing regions (and the RFLS systems have larger leading regions) of stratiform pre-

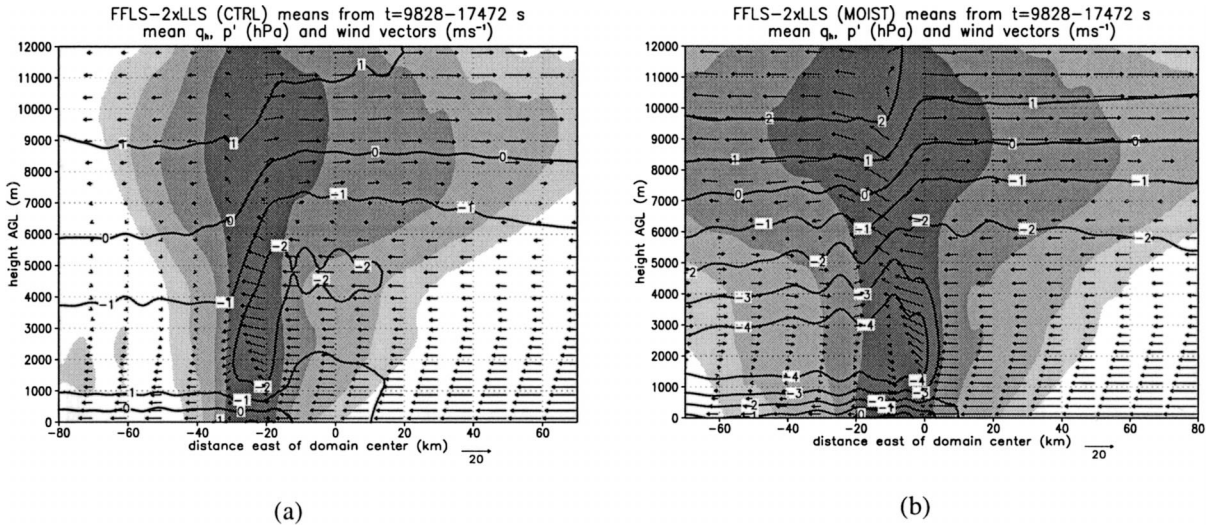

FIG. 19. Same as Fig. 12, but for FFLS–2xLLS simulations with (a) CTRL sounding and (b) MOIST sounding.

cipitation (rain rates >1 mm h^{-1} extended approximately 100 km from their convective lines, roughly consistent with their real-world counterparts). The physical explanation for the comparatively smaller leading stratiform precipitation regions in the FFLS(–2xLLS) simulations is as follows.

A variety of liquid and ice particles develop in the FFLS systems' convective updrafts and are transported into the downshear part of the convective system. Graupel particles with large terminal speeds fall out very near the line's position, melting as they descend below the 0° level and contributing to a core of moderate rainfall. Other ice and liquid particles that fall into the inflowing airstream are recirculated, eventually develop into larger graupel particles, and also fall out near the convective region. The remainder of the leading anvil in the middle and upper troposphere comprises snow, which falls very gradually over a much broader region. However, as these slowly falling particles descend below approximately 6 km AGL, they encounter a region of significant front-to-rear inflow (see Fig. 19) and are advected back toward the convective line, melting and evaporating all the while. In this way, the leading precipitation's horizontal extent at the surface is limited to a much smaller region than in the simulated RFLS or classical FFTS systems.

2) GOVERNING DYNAMICS

The basic low-level dynamics during the early parts (e.g., at $t = 119$ s) of the FFLS runs are nearly the same as those in the FFTS runs (e.g., in Fig. 14) owing to their identical 0–3-km wind profiles. However, as the first deep updraft ascends into the middle troposphere, notable differences begin to develop between the FFLS and FFTS MOIST simulations owing to the presence of 3–10-km shear in the FFLS environment. At $t = 833$ s, although the total p'_D remains approximately the same on the updrafts' downshear sides, it is far less strongly minimized on the upshear side of the FFLS updraft owing to the effect of the mean environmental shear (present in p'_{DL}). As a result, whereas the ACCB and ACCDNL fields continue to be similar to one another (Figs. 20c,d and 21c,d), significant downshear-directed ACCDL is present in the FFLS case and is absent from the FFTS case (Figs. 20e and 21e). In time, the integrated effects of this middle-tropospheric ACCDL contribute to the FFLS system's overturning updraft structure (much as in Fig. 19a).

The differences between the FFLS and FFLS–2xLLS simulations (as discussed above and shown in Fig. 18) also suggest that the 0–3-km shear is at least as important to the dynamics of organization as the mean 0–10-km shear. Comparing Fig. 14, which serves as a proxy for the FFLS simulation at $t = 119$ s, and Fig. 22, it is clear that an increase in low-level shear causes p'_{DL} to be more perturbed, and renders a larger downshear-directed ACCDL in the low levels (cf. Figs. 22e and 14e). Much as described earlier, this causes a still more erect cold-air nose with an even deeper and more upright low-level updraft (cf. Figs. 23 and 13a), giving air parcels a longer period of time to experience upward forcing and accumulate downshear ACCDL. As a result, the rearward-sloping low-level updraft in the FFTS and FFLS simulations is replaced by a draft with more nearly vertical momentum in the FFLS–2xLLS case, which then continues to acquire downshear ACCDL in the middle and upper troposphere owing to the presence of the 3–10-km shear.

On average, the pressure field in the mature simulated FFLS–2xLLS system was significantly per-

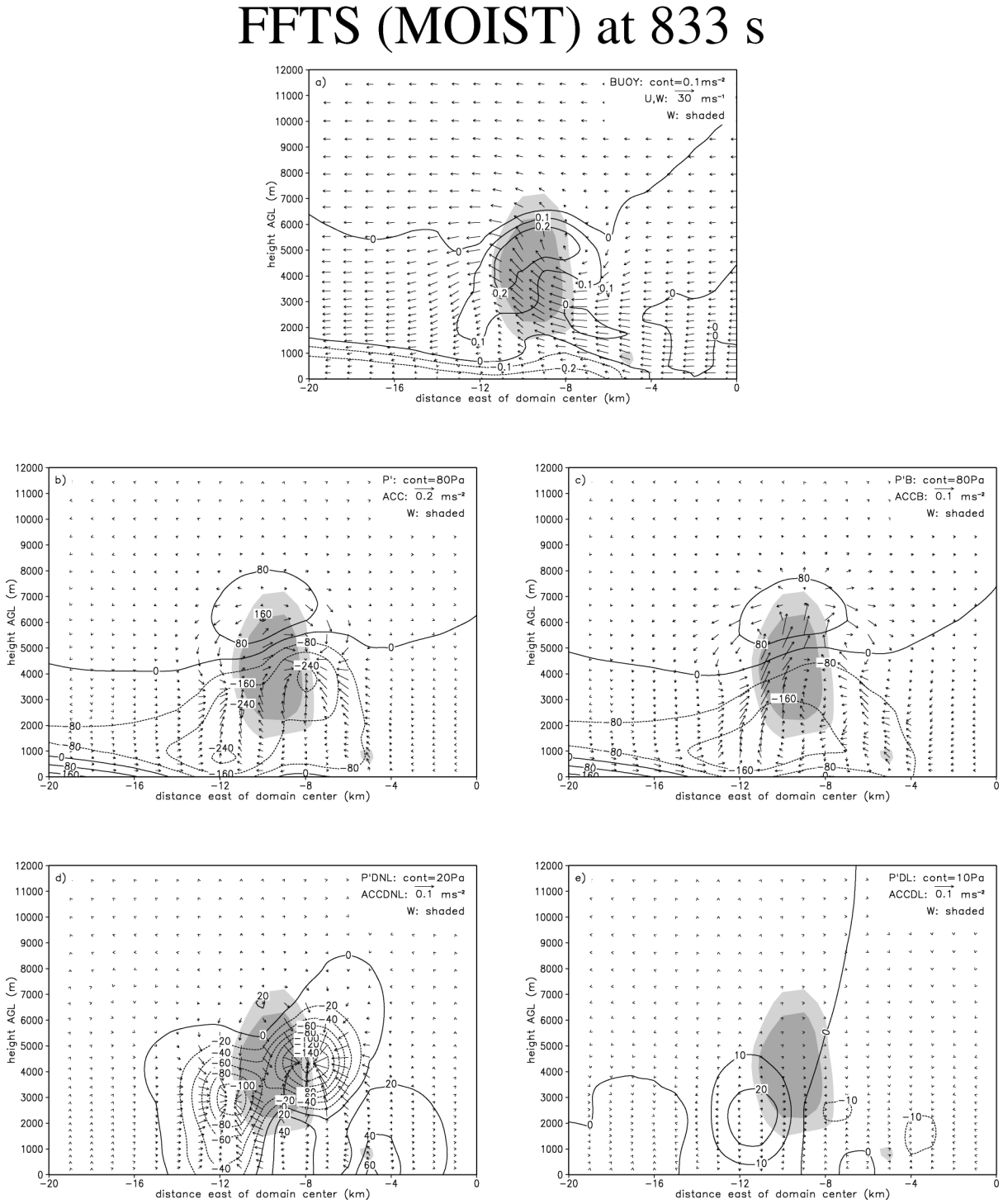

FIG. 20. Same as Fig. 14, but for simulation FFTS (MOIST) at 833 s, with W shaded at 5 and 10 m s^{-1}.

turbed on both sides of the convective region (Fig. 19a), which represents yet another departure from the classical conceptual model for an FFTS system [e.g., as described by Houze et al. (1989) and simulated in this study (Fig. 12a)]. A mean surface mesohigh exists to the west of $x = 0$ km in Fig. 19, and this is a quasi-hydrostatic response to the surface cold pool. In addition, a middle tropospheric mesolow exists to the east of the convective region (centered at about $x = 0$ km, $z = 4.5$ km AGL). This mesolow is largely a quasi-hydrostatic response to the latent heating and detrained buoyancy in the leading cloud and precip-

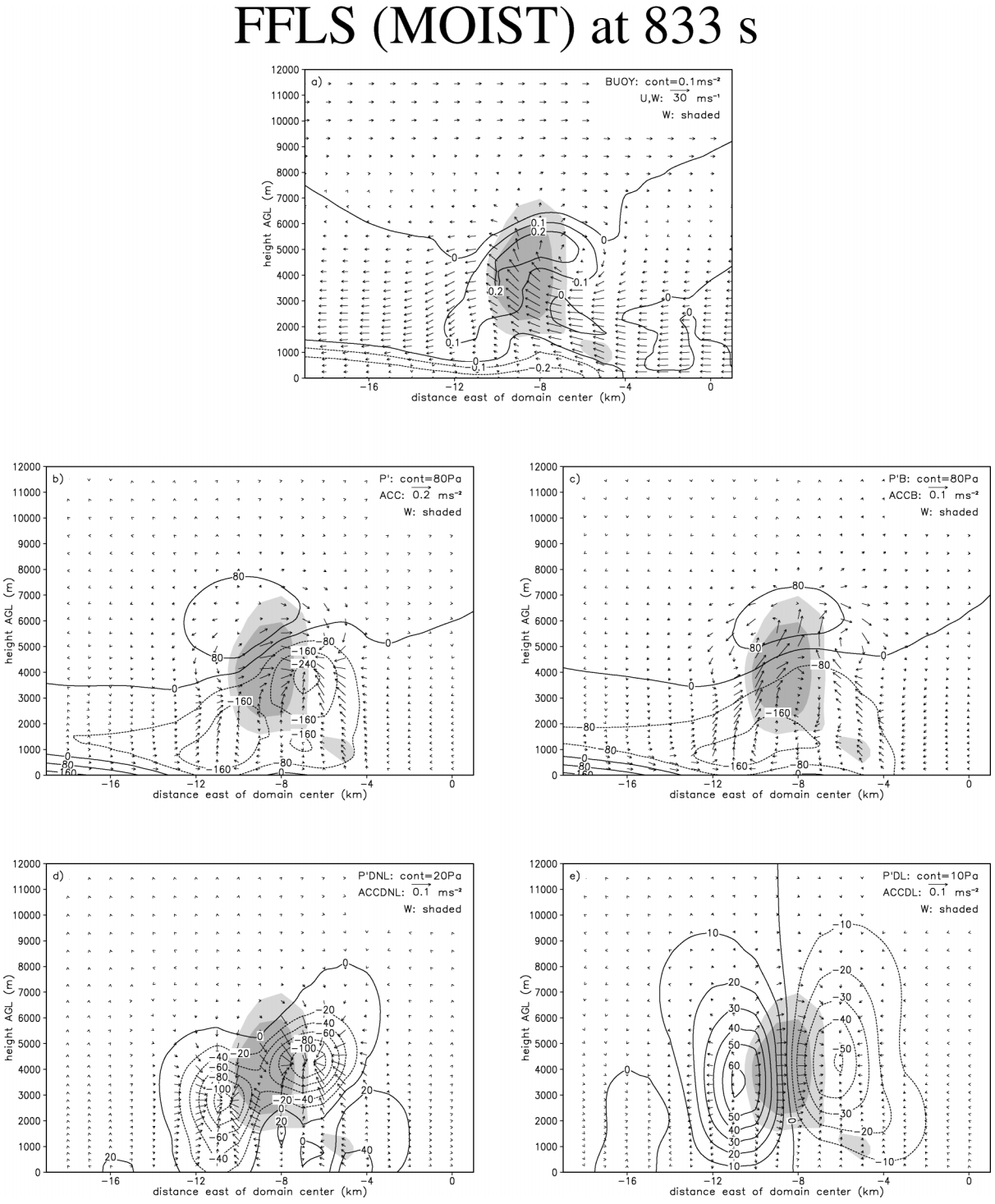

FIG. 21. Same as Fig. 14, but for simulation FFLS (MOIST) at 833 s, with W shaded at 5 and 10 m s^{-1}.

itation region. In this respect, it is analogous to the mesolows described for the FFTS and RFLS systems. Additionally, as discussed by Szeto and Cho (1994), there is a small dynamic contribution to the persistent mesolow (found in p'_{DNL}) owing to the curvature of the mean flow field. The importance of the FFLS system's unique pressure field is that middle-tropospheric environmental inflow is accelerated toward the convective line, thereby significantly modifying the near-line wind profile. Additionally, the upward pressure

FFLS–2xLLS (MOIST) at 119 s

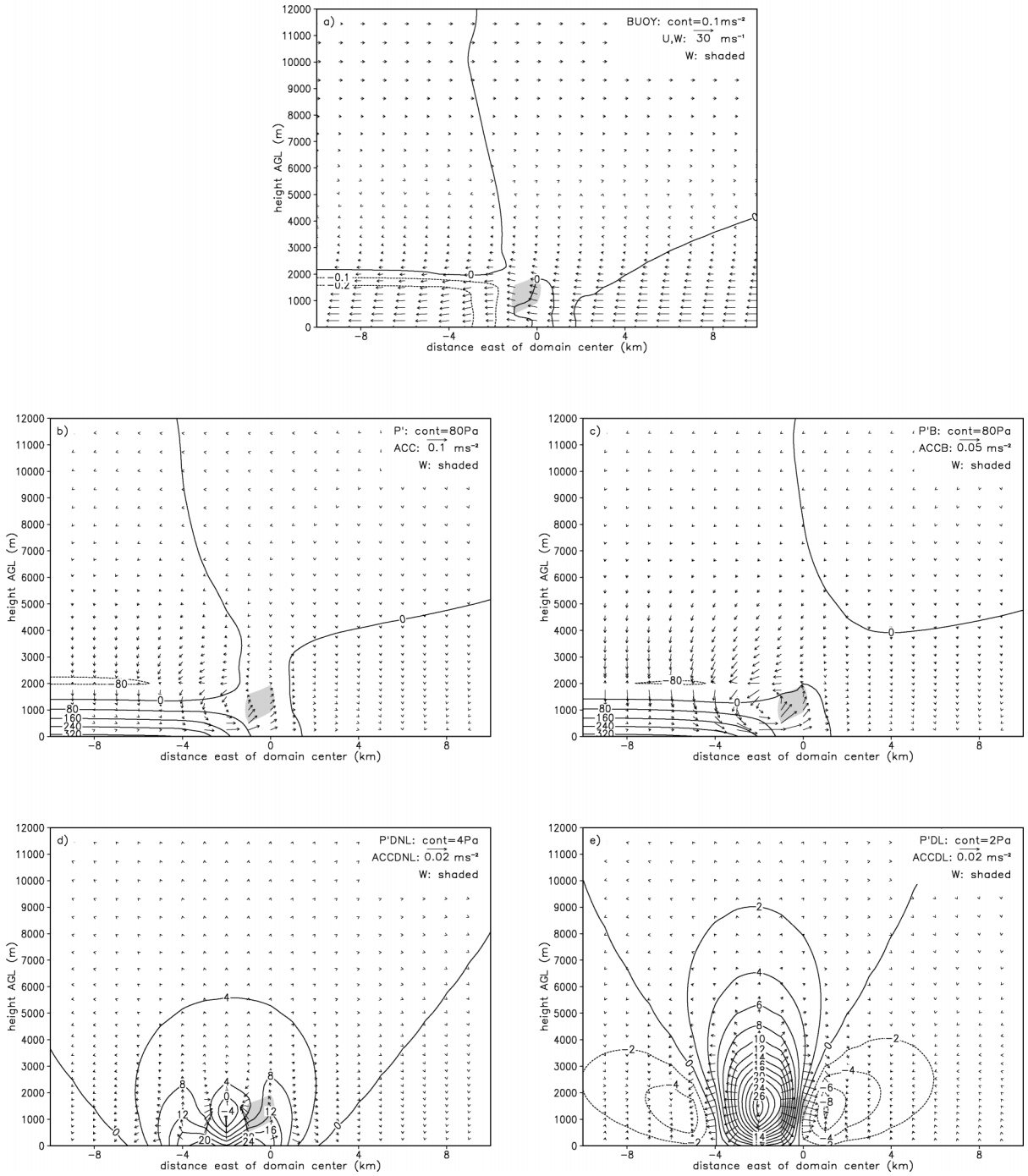

FIG. 22. Same as Fig. 14, but for simulation FFLS–2xLLS (MOIST) at 119 s.

gradient force owing to p' in the preline region can be important in providing upward accelerations to inflowing air parcels, whose ascent may help to continually destabilize the near-line environment.

5. Synthesis of results

Idealized 2D simulations can realistically reproduce the salient features of the hydrometeor and wind fields

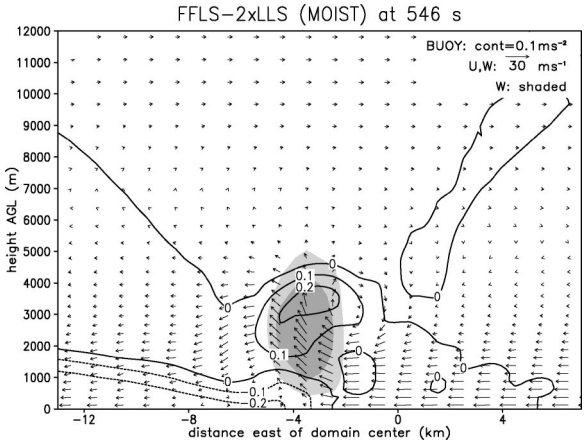

FIG. 23. Same as Fig. 13, but for FFLS–2xLLS (MOIST) simulation.

of the three quasi-2D linear MCS archetypes: FFTS, RFLS, and FFLS systems. We have proceeded to discuss the most basic dynamical principles that govern the organization of the systems into their respective modes in our idealized simulations with the presumption that the realistic looking modeled systems are physically similar to their real-world counterparts. The numerical results suggest that, to a large degree, the mesoscale organizational mode can be anticipated by considering the preferred direction of ACCB and ACCDL.

Near the edge of a surface cold pool, the buoyant pressure field slows the inflowing air, accelerates it upward for a period of time, and then accelerates it rapidly rearward over the cold pool and thereafter downward. In the case of the FFTS system on the downshear side of the cold pool, the linear dynamic pressure field associated with an updraft within mean environmental shear renders a downshear-directed ACCDL that opposes the rearward ACCB and renders a more upright and vigorous updraft. In the case of the RFLS system on the upshear side of the cold pool, ACCDL instead contributes an additional downshear, forward acceleration that renders trajectories with very shallow slopes. Indeed, in many cases (such as the CTRL sounding), deep convection will not develop in the basic RFLS setting. For this reason, RFLS systems are not the dynamical equivalent of a ''reversed FFTS system,'' despite their very similar reflectivity patterns and mesoscale flow features. The addition of reverse shear above a low-level jet in the RFLS setting (the RFLS-jet simulations) can render slightly more upright, vigorous updrafts owing to a rearward ACCDL in the middle troposphere, especially in tandem with an elevated, high θ_e inflow source; this point was previously noted by Fritsch et al. (1994). In the common setting of development on the downshear side of the surface cold pool, the addition of deep-layer shear (in this case, the 3–10-km layer) causes an overturning updraft structure owing to the downshear-directed ACCDL in the middle and upper troposphere. This addition can lead to an FFLS convective system in which air leaves the convective region with rear-to-fore momentum and carries hydrometeors into the leading precipitation region.

Our idealized simulations suggest that the deep-layer shear is an important part of the problem, but that the lower-tropospheric shear has a greater effect. These results are generally in accord with those of Rotunno et al. (1988), who analyzed the 2D dynamics of squall lines using horizontal vorticity. In optimal cases in which convective plumes are nearly upright, Rotunno et al. (1988) hypothesized that ''the import of positive vorticity associated with the low-level shear just balances the net buoyant generation of negative vorticity by the cold pool in the volume.'' Rotunno et al. (1988) also discussed deviations from this optimal state: when the import of low-level environmental vorticity is small or of the same sign as the baroclinic generation, cells should tilt or be swept downstream over the surface cold pool. When the import of low-level environmental vorticity is much larger than the baroclinic generation, cells should tilt or be swept downshear. These basic results are generally applicable to the quasi-2D MCS spectrum. Although it is unclear how, or if, Rotunno et al. (1988) incorporated the importance of the middle- and upper-tropospheric shear in discriminating between the FFTS and FFLS modes, Weisman (1992, 1993) did use their framework to discuss the sensitivity of MCS simulations to 0–5-km shear. Much as Lafore and Moncrieff (1989) suggested, a global view of MCS dynamics—including deep-layer shear and system-generated flow perturbations as well as local balance between the cold pool and low-level shear—seems best.

The idealized simulation results suggest predictability of quasi-2D linear MCS modes. For a particular situation, awareness of whether fresh convection is forming on the upshear or downshear side of a cold pool or baroclinic boundary, along with an assessment of the depth and strength of that shear, should enable one to anticipate whether the FFTS, RFLS, or FFLS organizational structure is most likely. PJ00 concluded that for the linear MCSs they studied, ''the stratiform precipitation arrangement . . . was roughly consistent with the advection of hydrometeors implied by the mean middle- and upper-tropospheric storm-relative winds.'' In part, that conclusion arose from the lack of statistically significant differences between the mean vertical wind shear for TS and LS MCSs. One strong possibility is that, because PJ00 included both RFLS and FFLS systems within one unified category based upon their reflectivity structure, the weak deep-layer shear of the RFLS systems and the strong deep-layer shear of the FFLS systems were averaged into one relatively undistinctive profile. From an acceleration perspective, it must be differences in vertical wind shear that account for the different structures, as a result of the direct impact of the magnitude of the environmental shear upon the linear part of the dynamic pressure perturbation.

6. Indicated future work

Given that our lack of data provided significant motivation for the idealized modeling approach that we used in the present study, it would be well to perform similar analyses of archetypal cases with high-quality dual-Doppler radar datasets and research-quality near-system soundings. Additionally, although we have outlined the basic similarities of RFLS to FFTS systems, there exist some notable and unique features of the typical RFLS system that we did not attempt to simulate in our idealized experiments. In what way might a stable nocturnal layer paired with an elevated maximum in humidity and θ_e interact with a preexisting linear boundary? Could such a regime avoid the large downshear accelerations in the lower troposphere that can prevent deep convection from developing on a cold pool's upshear side? Real world studies and more complicated simulations would be useful in addressing such questions. Likewise, the uniqueness of FFLS MCSs among quasi-2D systems commends them for additional study. In addition to the basic dynamic perspective in the present paper, there appear to exist additional positive feedbacks that reinforce the downshear accelerations in FFLS systems. It also appears that FFLS systems can survive the seeming contamination of their inflow by the line-leading precipitation because ascent and diabatic cooling in the LS region can destabilize the inflowing airstream. To these ends, we are preparing additional papers that will address the dynamics, maintenance, and sensitivities of FFLS systems in greater detail than was possible in this overview paper. Finally, in this paper we have focused exclusively on quasi-2D linear convective systems. Investigation of convective lines with parallel stratiform precipitation remains to be done. Given their somewhat unique three-dimensional structure and significant along-line flow fields, their dynamics are likely yet again distinct from those of all the quasi-2D systems. As in this study, idealized numerical simulations may provide a first glimpse into the dynamics that govern their organization and evolution.

7. Summary

In this paper we presented together the three commonly observed modes of quasi-2D linear convective systems. We reviewed prior observations of front-fed convective lines with trailing stratiform precipitation (FFTS) and rear-fed convective lines with leading stratiform precipitation (RFLS), and then presented some observations and a basic consolidated conceptual model for front-fed convective lines with leading stratiform precipitation (FFLS). All three modes were reasonably well simulated in two dimensions. Our idealized simulations suggest that the magnitude of the low-level and deep-layer shear vectors, and their orientation with respect to a cold pool or baroclinic boundary, is of first importance in determining which of the quasi-2D convective modes will develop. This basic framework also helps to distinguish RFLS systems from simple mirror images of FFTS systems. Given the somewhat more complicated structure and maintenance of the FFLS systems, we are working on addressing their dynamics in greater detail than was possible here.

Acknowledgments. The authors thank G. Cordova and R. Taft of Colorado State University (CSU) for their assistance throughout this work. We gratefully acknowledge the suggestions and contributions of M. Moncrieff, C. Pettet, and M. Weisman of the National Center for Atmospheric Research (NCAR). The simulations in this study were made using the Advanced Regional Prediction System (ARPS) developed by the Center for Analysis and Prediction of Storms (CAPS), University of Oklahoma. CAPS is supported by the National Science Foundation (NSF) and the Federal Aviation Administration through combined Grant ATM92-20009. NCAR provided supercomputer facilities and computational time for many of the simulations in this study. NSF funded this research under Grant ATM-0071371.

REFERENCES

Blanchard, D. O., 1990: Mesoscale convective patterns of the southern High Plains. *Bull. Amer. Meteor. Soc.,* **71,** 994–1005.

Bluestein, H. B., and M. H. Jain, 1985: Formation of mesoscale lines of precipitation: Severe squall lines in Oklahoma during the spring. *J. Atmos. Sci.,* **42,** 1711–1732.

Doswell, C. A., III, H. E. Brooks, and R. A. Maddox, 1996: Flash flood forecasting: An ingredients-based methodology. *Wea. Forecasting,* **11,** 560–581.

Fankhauser, J. C., G. M. Barnes, and M. A. LeMone, 1992: Structure of a midlatitude squall line formed in strong unidirectional shear. *Mon. Wea. Rev.,* **120,** 237–260.

Fovell, R. G., and P.-H. Tan, 1998: The temporal behavior of numerically simulated multicell-type storms. Part II: The convective cell life cycle and cell regeneration. *Mon. Wea. Rev.,* **126,** 551–577.

Fritsch, J. M., and G. S. Forbes, 2001: Mesoscale convective systems. *Severe Convective Storms, Meteor. Monogr.,* No. 50, Amer. Meteor. Soc., 323–357.

——, J. D. Murphy, and J. S. Kain, 1994: Warm-core vortex amplification over land. *J. Atmos. Sci.,* **51,** 1780–1807.

Grady, R. L., and J. Verlinde, 1997: Triple-Doppler analysis of a discretely propagating, long-lived, High Plains squall line. *J. Atmos. Sci.,* **54,** 2729–2748.

Houze, R. A., Jr., and E. N. Rappaport, 1984: Air motions and precipitation structure of an early summer squall line over the eastern tropical Atlantic. *J. Atmos. Sci.,* **41,** 553–574.

——, S. A. Rutledge, M. I. Biggerstaff, and B. F. Smull, 1989: Interpretation of Doppler weather radar displays of midlatitude mesoscale convective systems. *Bull. Amer. Meteor. Soc.,* **70,** 608–619.

——, B. F. Smull, and P. Dodge, 1990: Mesoscale organization of springtime rainstorms in Oklahoma. *Mon. Wea. Rev.,* **118,** 613–654.

Kessinger, C. J., P. S. Ray, and C. E. Hane, 1987: The Oklahoma squall line of 19 May 1977. Part I: A multiple Doppler analysis of convective and stratiform structure. *J. Atmos. Sci.,* **44,** 2840–2864.

Klemp, J. B., 1987: Dynamics of tornadic thunderstorms. *Annu. Rev. Fluid Mech.,* **19,** 369–402.

Lafore, J.-P., and M. W. Moncrieff, 1989: A numerical investigation

of the organization and interaction of the convective and stratiform regions of tropical squall lines. *J. Atmos. Sci.,* **46,** 521–544.

Laing, A. G., and J. M. Fritsch, 1997: The global population of mesoscale convective complexes. *Quart. J. Roy. Meteor. Soc.,* **123,** 389–405.

Lin, Y.-L., R. D. Farley, and H. D. Orville, 1983: Bulk parameterization of the snow field in a cloud model. *J. Climate Appl. Meteor.,* **22,** 1065–1092.

——, R. L. Deal, and M. S. Kulie, 1998: Mechanisms of cell regeneration, development, and propagation within a two-dimensional multicell storm. *J. Atmos. Sci.,* **55,** 1867–1886.

Maddox, R. A., C. F. Chappell, and L. R. Hoxit, 1979: Synoptic and meso-α scale aspects of flash flood events. *Bull. Amer. Meteor. Soc.,* **60,** 115–123.

Moncrieff, M. W., 1992: Organized convective systems: Archetypal dynamical models, mass and momentum flux theory, and parameterization. *Quart. J. Roy. Meteor. Soc.,* **118,** 819–850.

——, and C. Liu, 1999: Convective initiation by density currents: Role of convergence, shear, and dynamical organization. *Mon. Wea. Rev.,* **127,** 2455–2464.

Nachamkin, J. E., R. L. McAnelly, and W. R. Cotton, 2000: Interactions between a developing mesoscale convective system and its environment. Part I: Observational analysis. *Mon. Wea. Rev.,* **128,** 1205–1224.

Newton, C. W., 1950: Structure and mechanism of the prefrontal squall line. *J. Meteor.,* **7,** 210–222.

——, and J. C. Fankhauser, 1964: On the movements of convective storms, with emphasis on size discrimination in relation to water-budget requirements. *J. Appl. Meteor.,* **3,** 651–668.

Nicholls, M. E., R. H. Johnson, and W. R. Cotton, 1988: The sensitivity of two-dimensional simulations of tropical squall lines to environmental profiles. *J. Atmos. Sci.,* **45,** 3625–3649.

Ogura, Y., and M.-T. Liou, 1980: The structure of a midlatitude squall line: A case study. *J. Atmos. Sci.,* **37,** 553–567.

Parker, M. D., and R. H. Johnson, 2000: Organizational modes of midlatitude mesoscale convective systems. *Mon. Wea. Rev.,* **128,** 3413–3436.

——, S. A. Rutledge, and R. H. Johnson, 2001: Cloud-to-ground lighting in linear mesoscale convective systems. *Mon. Wea. Rev.,* **129,** 1232–1242.

Pettet, C. R., 2001: Airflow and precipitation structure of two leading stratiform mesoscale convective systems. M.S. thesis, Department of Atmospheric Science, Colorado State University, 106 pp. [Available from Department of Atmospheric Science, Colorado State University, Fort Collins, CO 80523-1371.]

——, and R. H. Johnson, 2003: Airflow and precipitation structure of two leading stratiform mesoscale convective systems determined from operational datasets. *Wea. Forecasting,* **18,** 685–699.

Rotunno, R., and J. B. Klemp, 1982: The influence of the shear-induced pressure gradient on thunderstorm motion. *Mon. Wea. Rev.,* **110,** 136–151.

——, ——, and M. L. Weisman, 1988: A theory for strong, long-lived squall lines. *J. Atmos. Sci.,* **45,** 463–485.

Rutledge, S. A., R. A. Houze Jr., M. I. Biggerstaff, and T. Matejka, 1988: The Oklahoma–Kansas mesoscale convective system of 10–11 June 1985: Precipitation structure and single-Doppler radar analysis. *Mon. Wea. Rev.,* **116,** 1409–1430.

Schiesser, H. H., R. A. Houze Jr., and H. Huntreiser, 1995: The mesoscale structure of severe precipitation systems in Switzerland. *Mon. Wea. Rev.,* **123,** 2070–2097.

Seitter, K. L., and H.-L. Kuo, 1983: The dynamical structure of squall-line type thunderstorms. *J. Atmos. Sci.,* **40,** 2831–2854.

Skamarock, W. C., M. L. Weisman, and J. B. Klemp, 1994: Three-dimensional evolution of simulated long-lived squall lies. *J. Atmos. Sci.,* **51,** 2563–2584.

Smull, B. F., and R. A. Houze Jr., 1985: A midlatitude squall line with a trailing region of stratiform rain: Radar and satellite observations. *Mon. Wea. Rev.,* **113,** 117–133.

——, and ——, 1987: Dual-Doppler radar analysis of a midlatitude squall line with a trailing region of stratiform rain. *J. Atmos. Sci.,* **44,** 2128–2148.

Szeto, K. K., and H.-R. Cho, 1994: A numerical investigation of squall lines. Part II: The mechanics of evolution. *J. Atmos. Sci.,* **51,** 425–433.

Tao, W.-K., and J. Simpson, 1993: Goddard Cumulus Ensemble Model. Part I: Model description. *Terr. Atmos. Oceanic Sci.,* **4,** 35–72.

Thorpe, A. J., M. J. Miller, and M. W. Moncrieff, 1982: Two-dimensional convection in non-constant shear: A model of midlatitude squall lines. *Quart. J. Roy. Meteor. Soc.,* **108,** 739–762.

Weisman, M. L., 1992: The role of convectively generated rear-inflow jets in the evolution of long-lived mesoconvective systems. *J. Atmos. Sci.,* **49,** 1826–1847.

——, 1993: The genesis of severe, long-lived bow echoes. *J. Atmos. Sci.,* **50,** 645–670.

——, and J. B. Klemp, 1982: The dependence of numerically simulated convective storms on vertical wind shear and buoyancy. *Mon. Wea. Rev.,* **110,** 504–520.

——, ——, and R. Rotunno, 1988: Structure and evolution of numerically simulated squall lines. *J. Atmos. Sci.,* **45,** 1990–2013.

——, W. C. Skamarock, and J. B. Klemp, 1997: The resolution dependence of explicitly modeled convective systems. *Mon. Wea. Rev.,* **125,** 527–548.

Wilhelmson, R. B., and Y. Ogura, 1972: The pressure perturbation and the numerical modelling of a cloud. *J. Atmos. Sci.,* **29,** 1295–1307.

Xue, M., K. K. Doregemeier, V. Wong, A. Shapiro, and K. Brewster, 1995: Advanced Regional Prediction System version 4.0 users guide. Center for the Analysis and Prediction of Storms, Norman, OK, 380 pp. [Available from ARPS Model Development Group, CAPS, University of Oklahoma, 100 East Boyd, Norman, OK 73019-0628.]

——, ——, and ——, 2000: The Advanced Regional Prediction System (ARPS)—A multiscale nonhydrostatic atmospheric simulation and prediction tool. Part I: Model dynamics and verification. *Meteor. Atmos. Phys.,* **75,** 161–193.

——, and Coauthors, 2001: The Advanced Regional Prediction System (ARPS)—A multiscale nonhydrostatic atmospheric simulation and prediction tool. Part II: Model physics and applications. *Meteor. Atmos. Phys.,* **76,** 134–165.

Yang, M.-J., and R. A. Houze Jr., 1995: Multicell squall-line structure as a manifestation of vertically trapped gravity waves. *Mon. Wea. Rev.,* **123,** 641–661.